TeV Halos:

A New Class of Gamma-Ray Sources Provide Insight into Galactic Diffusion

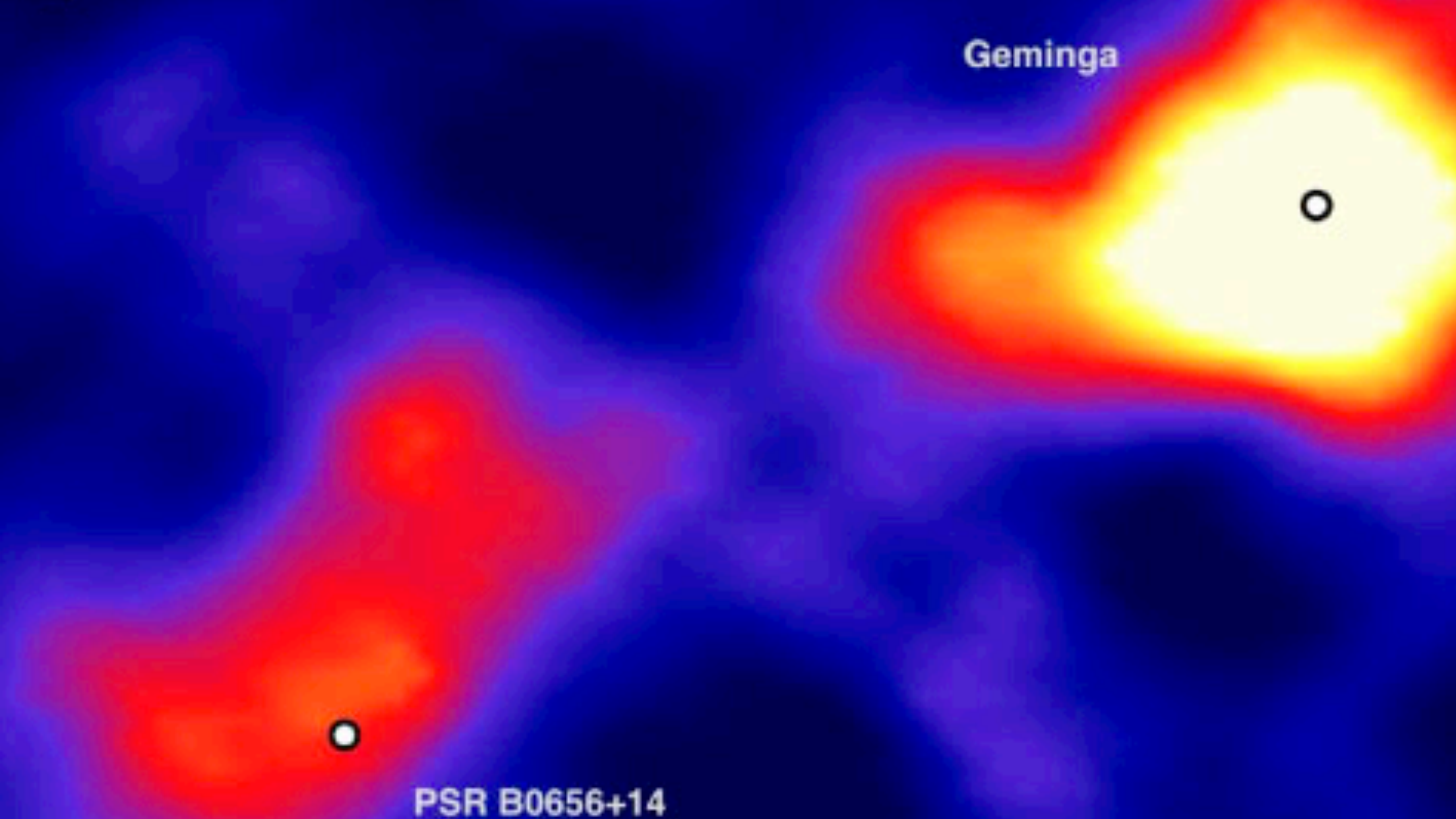Geminga

PSR B0656+14

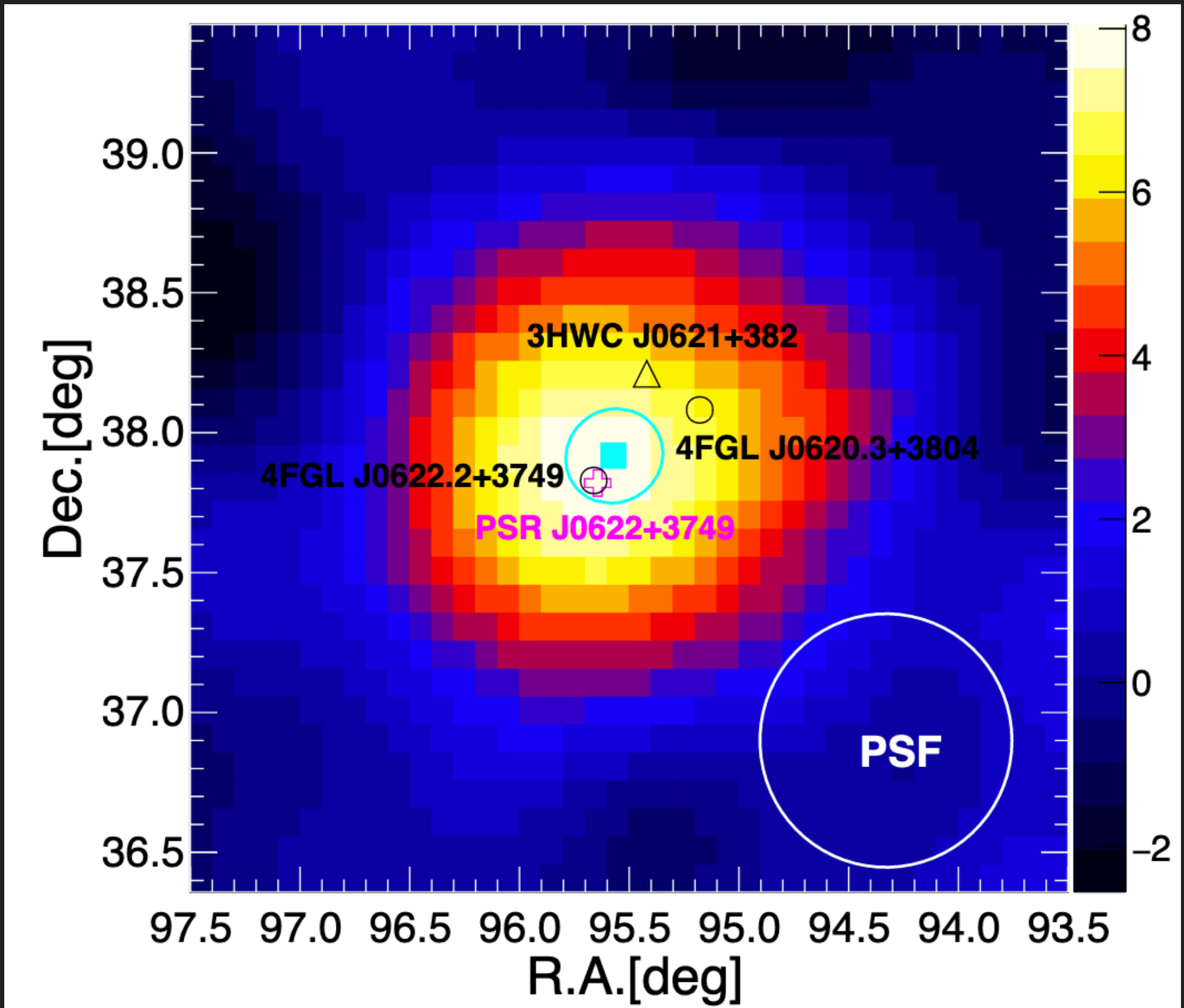TIM LINDEN

Stockholm University

Geminga

PSR B0656+14

▸ TeV Halos (Observationally):

  ▸ At least 7 detected systems (potentially dozens)

  ▸ Detected by all instruments (HAWC, LHAASO, HESS, VERITAS)

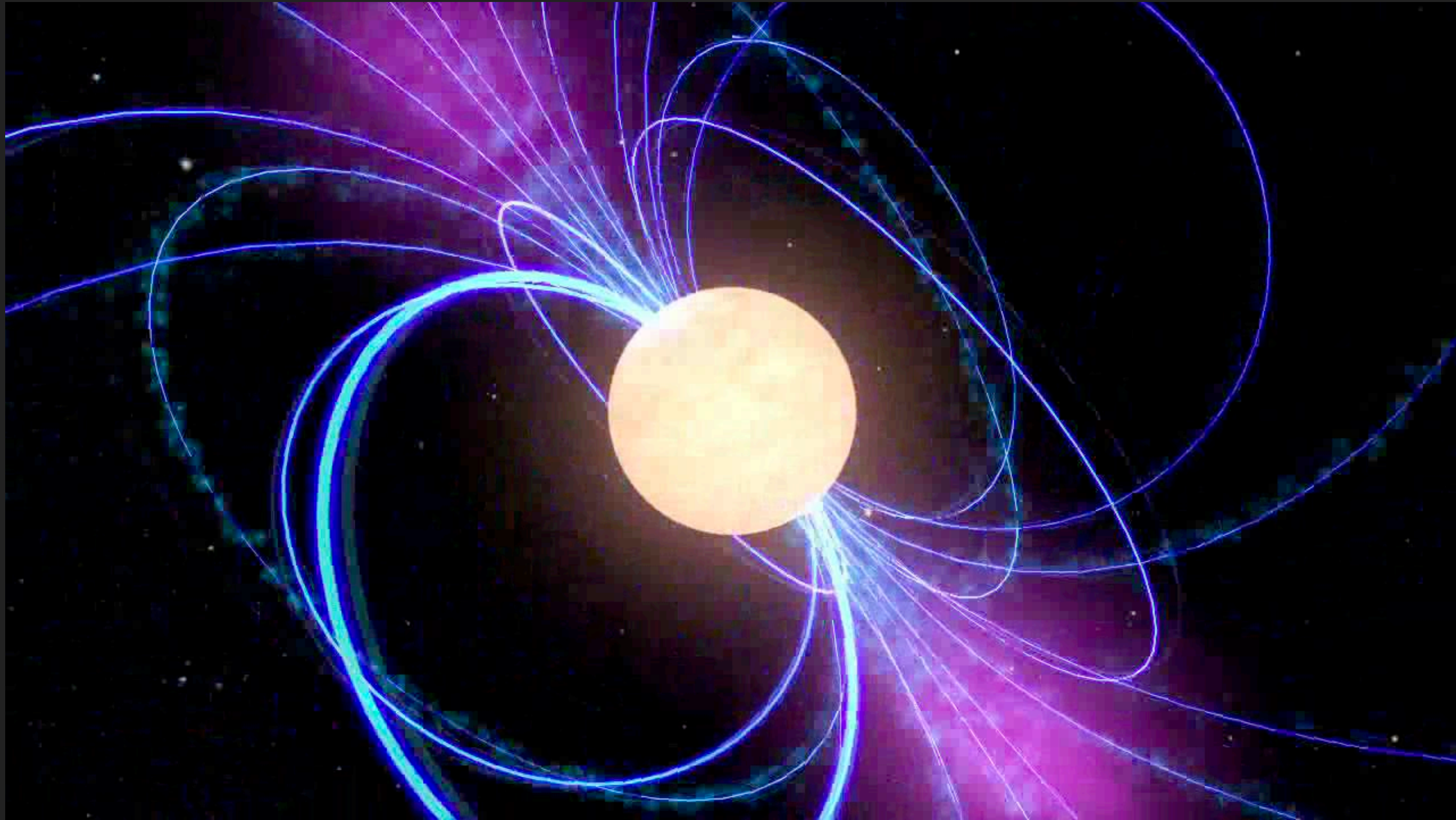 ▸ Detected systems are nearby, or have high spin down power.

ATNF Name	Dec. (°)	Distance (kpc)	Age (kyr)	Spindown Lum. (erg s^{-1})	Spindown Flux (erg s^{-1} kpc^{-2})	2HWC
J0633+1746	17.77	0.25	342	3.2e34	4.1e34	2HWC J0631+169
B0656+14	14.23	0.29	111	3.8e34	3.6e34	2HWC J0700+143
B1951+32	32.87	3.00	107	3.7e36	3.3e34	—
J1740+1000	10.00	1.23	114	2.3e35	1.2e34	—
J1913+1011	10.18	4.61	169	2.9e36	1.1e34	2HWC J1912+099
J1831-0952	-9.86	3.68	128	1.1e36	6.4e33	2HWC J1831-098
J2032+4127	41.45	1.70	181	1.7e35	4.7e33	2HWC J2031+415
B1822-09	-9.58	0.30	232	4.6e33	4.1e33	—
B1830-08	-8.45	4.50	147	5.8e35	2.3e33	—
J1913+0904	9.07	3.00	147	1.6e35	1.4e33	—
B0540+23	23.48	1.56	253	4.1e34	1.4e33	—

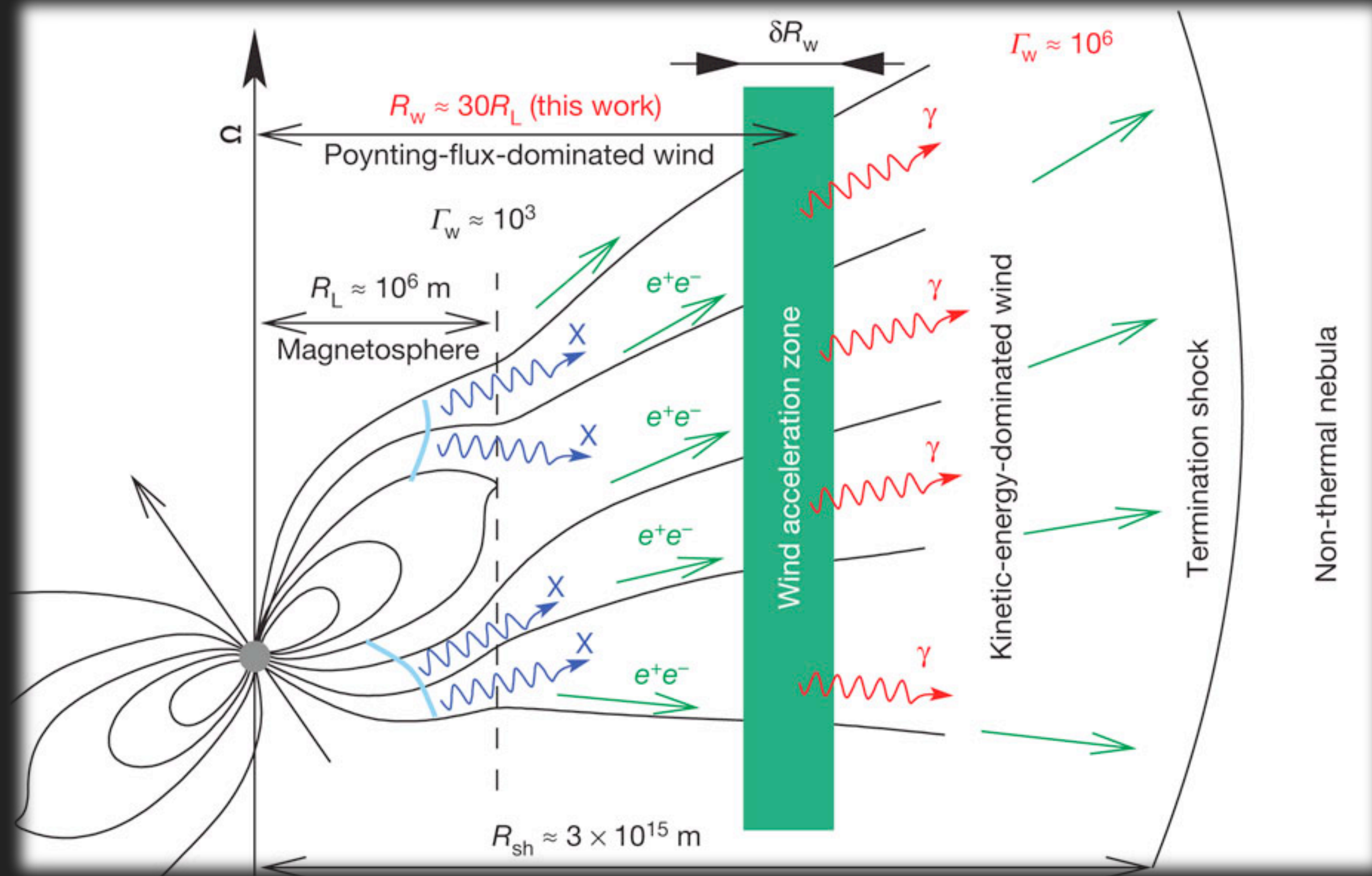| ATNF Name	Dec. (°)	Distance (kpc)	Age (kyr)	Spindown Lum. (erg s^{-1})	Spindown Flux (erg s^{-1} kpc^{-2})	2HWC
J0633+1746	17.77	0.25	342	3.2e34	4.1e34	2HWC J0631+169
B0656+14	14.23	0.29	111	3.8e34	3.6e34	2HWC J0700+143
B1951+32	32.87	3.00	107	3.7e36	3.3e34	—
J1740+1000	10.00	1.23	114	2.3e35	1.2e34	—
J1913+1011	10.18	4.61	169	2.9e36	1.1e34	2HWC J1912+099
J1831-0952	-9.86	3.68	128	1.1e36	6.4e33	2HWC J1831-098
J2032+4127	41.45	1.70	181	1.7e35	4.7e33	2HWC J2031+415
B1822-09	-9.58	0.30	232	4.6e33	4.1e33	—
B1830-08	-8.45	4.50	147	5.8e35	2.3e33	—
J1913+0904	9.07	3.00	147	1.6e35	1.4e33	—
B0540+23	23.48	1.56	253	4.1e34	1.4e33	—

▸ TeV Halos require a large fraction of the total spin down power to be converted into gamma-rays.

▸ Geminga flux is 3×10^{-13} TeV cm^{-2}s^{-1} at 7 TeV, corresponds to more than 0.1% of spin down power.

‣Rotational Kinetic Energy of the neutron star is the <u>ultimate power source</u> of all emission in this problem.

- Electrons boiled off the surface of the pulsar produce a cascade of e+e- pairs.

ATNF Name	Dec. ($^\circ$)	Distance (kpc)	Age (kyr)	Spindown Lum. (erg s^{-1})	Spindown Flux (erg s^{-1} kpc^{-2})	2HWC
J0633+1746	17.77	0.25	342	3.2e34	4.1e34	2HWC J0631+169
B0656+14	14.23	0.29	111	3.8e34	3.6e34	2HWC J0700+143
B1951+32	32.87	3.00	107	3.7e36	3.3e34	—
J1740+1000	10.00	1.23	114	2.3e35	1.2e34	—
J1913+1011	10.18	4.61	169	2.9e36	1.1e34	2HWC J1912+099
J1831-0952	-9.86	3.68	128	1.1e36	6.4e33	2HWC J1831-098
J2032+4127	41.45	1.70	181	1.7e35	4.7e33	2HWC J2031+415
B1822-09	-9.58	0.30	232	4.6e33	4.1e33	—
B1830-08	-8.45	4.50	147	5.8e35	2.3e33	—
J1913+0904	9.07	3.00	147	1.6e35	1.4e33	—
B0540+23	23.48	1.56	253	4.1e34	1.4e33	—

- Geminga flux is 3×10^{-13} TeV cm^{-2}s^{-1} at 7 TeV, corresponds to more than 0.1% of spin down power.

- For a standard inverse-Compton scattering model, this indicates that 10% of the spin down power is converted into e+e- pairs.
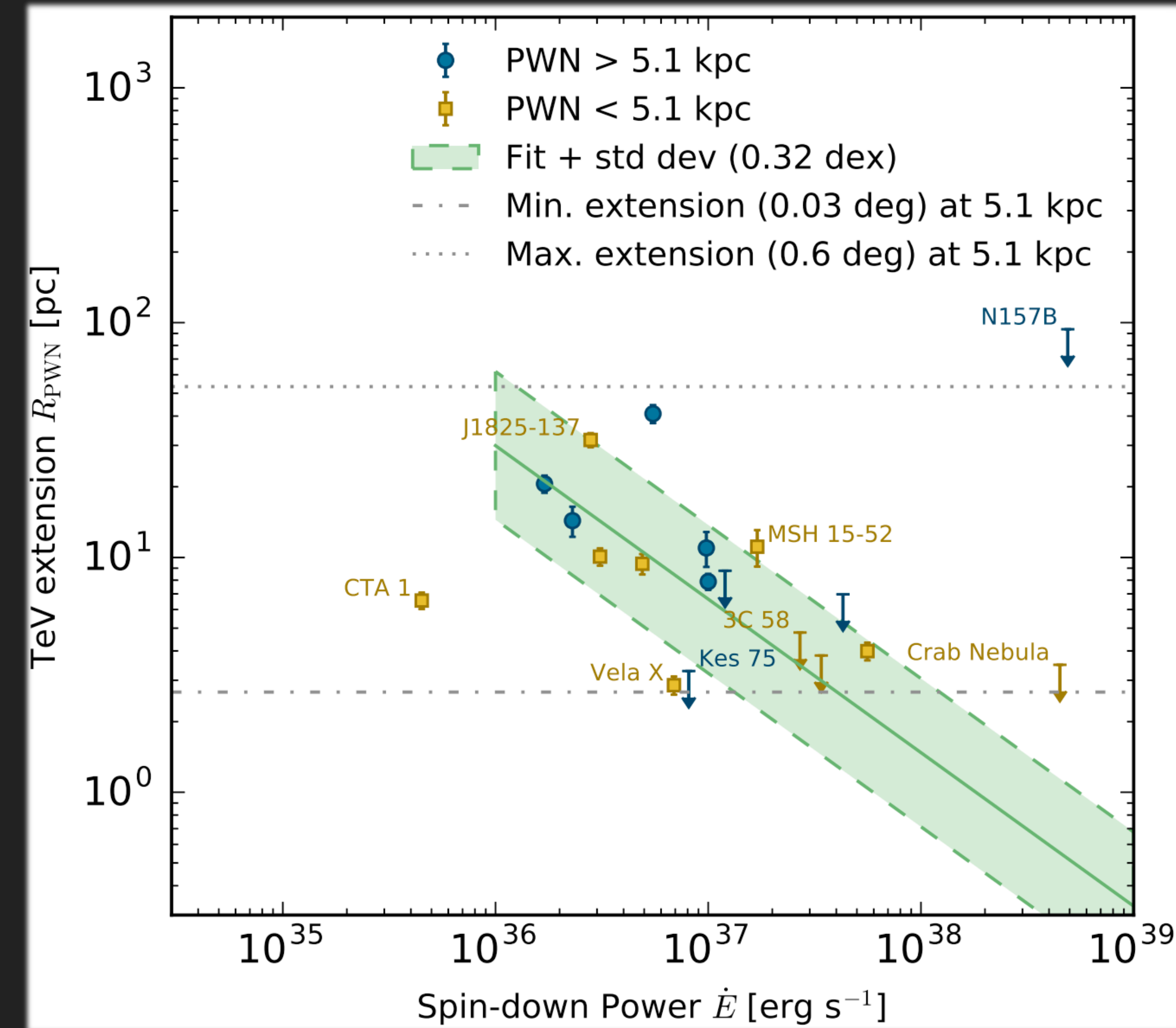
TeV Halos are much larger than PWN, especially at low spin down energies and large ages.

But much smaller than expected if TeV electrons were just propagating through the interstellar medium.

NOTE: The size of halos has the opposite time-dependence as the X-Ray PWN.

$$R_{\mathrm{PWN}} \simeq 1.5 \left(\frac{\dot{E}}{10^{35}\,\mathrm{erg/s}} \right)^{1/2} \times$$
$$\left(\frac{n_{\mathrm{gas}}}{1\,\mathrm{cm}^{-3}} \right)^{-1/2} \left(\frac{v}{100\,\mathrm{km/s}} \right)^{-3/2} \mathrm{pc}$$

EARLY LESSONS

- **1.) Pulsars are highly efficient e^+e^- accelerators.**

- **2.) Pulsar e^+e^- are not confined in the source.**

- **3.) Regions near sources have unusually low diffusion coefficients.**

Geminga

PSR B0656+14

ATNF Name	Dec. (°)	Distance (kpc)	Age (kyr)	Spindown Lum. (erg s^{-1})	Spindown Flux (erg s^{-1} kpc^{-2})	2HWC
J0633+1746	17.77	0.25	342	3.2e34	4.1e34	2HWC J0631+169
B0656+14	14.23	0.29	111	3.8e34	3.6e34	2HWC J0700+143
B1951+32	32.87	3.00	107	3.7e36	3.3e34	—
J1740+1000	10.00	1.23	114	2.3e35	1.2e34	—
J1913+1011	10.18	4.61	169	2.9e36	1.1e34	2HWC J1912+099
J1831-0952	-9.86	3.68	128	1.1e36	6.4e33	2HWC J1831-098
J2032+4127	41.45	1.70	181	1.7e35	4.7e33	2HWC J2031+415
B1822-09	-9.58	0.30	232	4.6e33	4.1e33	—
B1830-08	-8.45	4.50	147	5.8e35	2.3e33	—
J1913+0904	9.07	3.00	147	1.6e35	1.4e33	—
B0540+23	23.48	1.56	253	4.1e34	1.4e33	—

▸ **Make One Key Assumption:**

▸ **The following correlation is consistent with the data.**
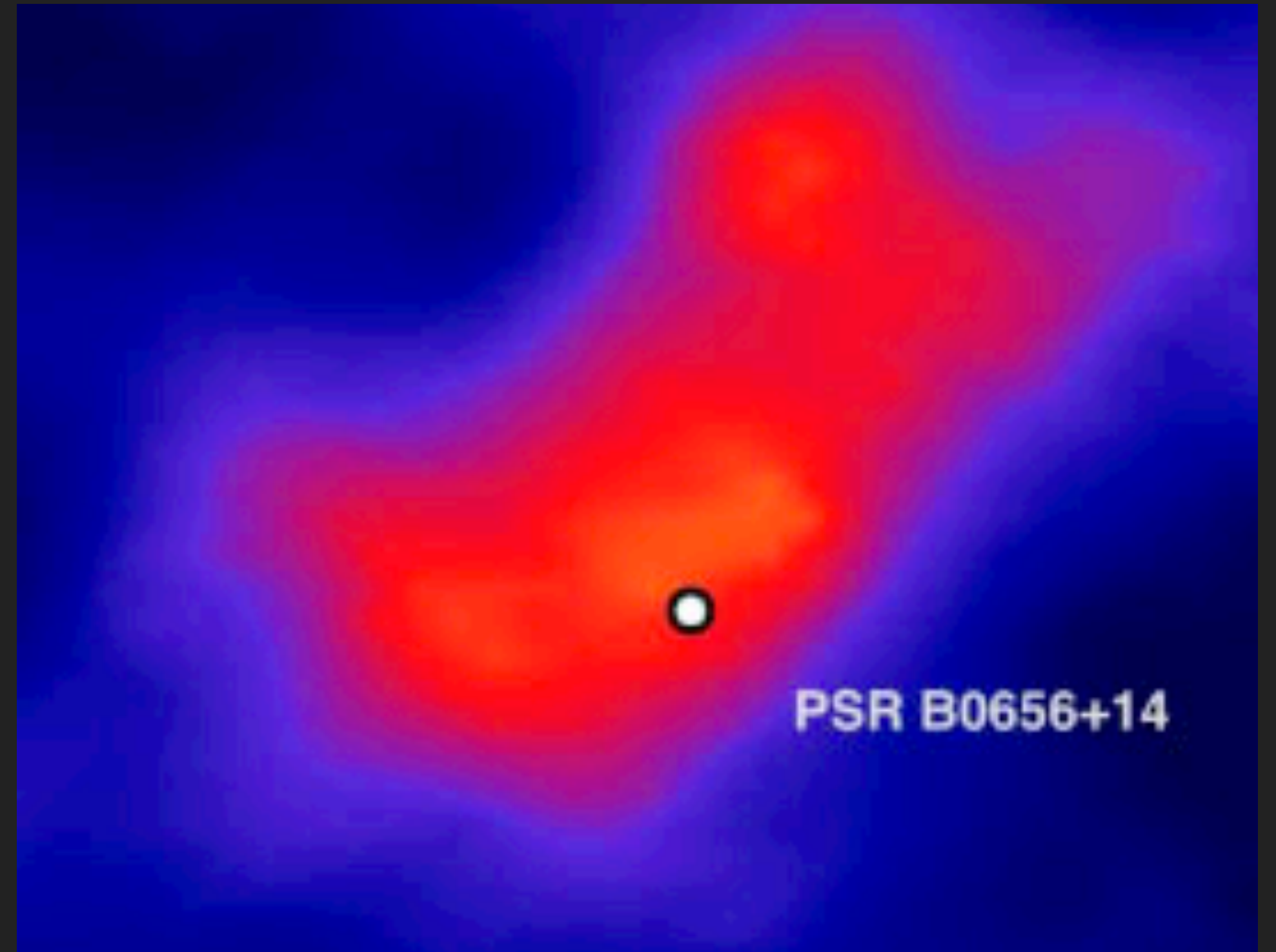
$$\phi_{\text{TeV halo}} = \left(\frac{\dot{E}_{\text{psr}}}{\dot{E}_{\text{Geminga}}} \right) \left(\frac{d^2_{\text{Geminga}}}{d^2_{\text{psr}}} \right) \phi_{\text{Geminga}}$$

▸ **Note: Using Monogem would increases fluxes by nearly a factor of 2. The power law of this correlation doesn't greatly affect the results.**

PWN

PSR B0656+14

TeV Halo

# DIFFERENCES IN DEFINITION - GOING BEYOND THE GEMINGA-MODEL

- An alternative definition of a "TeV halo" is used by Giacinti et al. 2019 (1907.12121)

- Linden et al. (2017) - A TeV halo is a leptonic gamma-ray source surrounding a pulsar, where the electrons are diffusing through the medium (rather than being driven by convective pulsar winds).

- Giacinti et al. (2019) - A TeV halo is a leptonic gamma-ray source surrounding a pulsar, where the emission stems from a region where the electron density falls below the ambient ISM electron density.
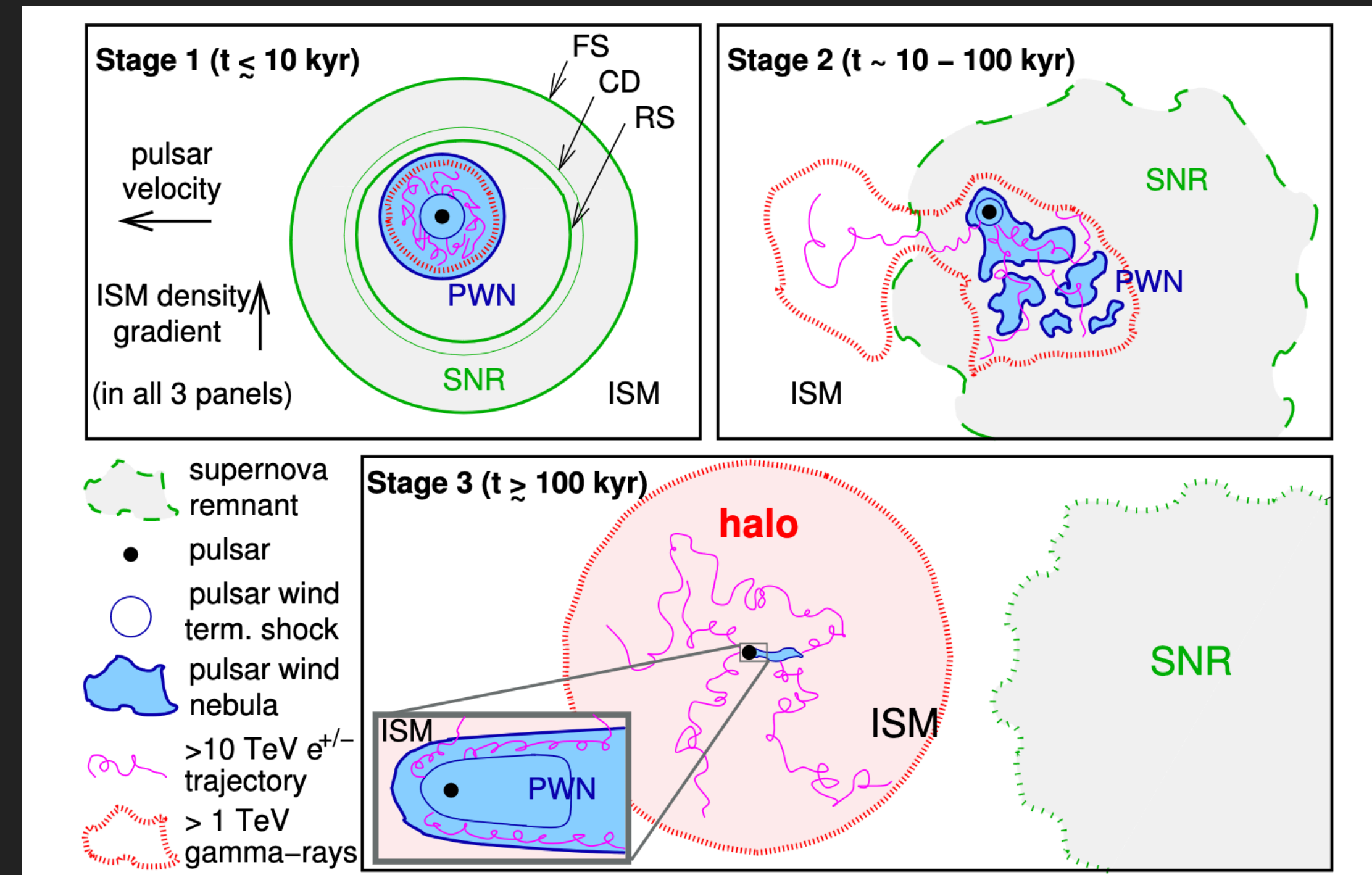
Di Mauro, Manconi, Donato (2019; 1908.03216)

- In particular, this extended diffusive halos have been found in a number of young systems.

- Inhibited diffusion appears to occur very soon after system formation, and persist for a long time.
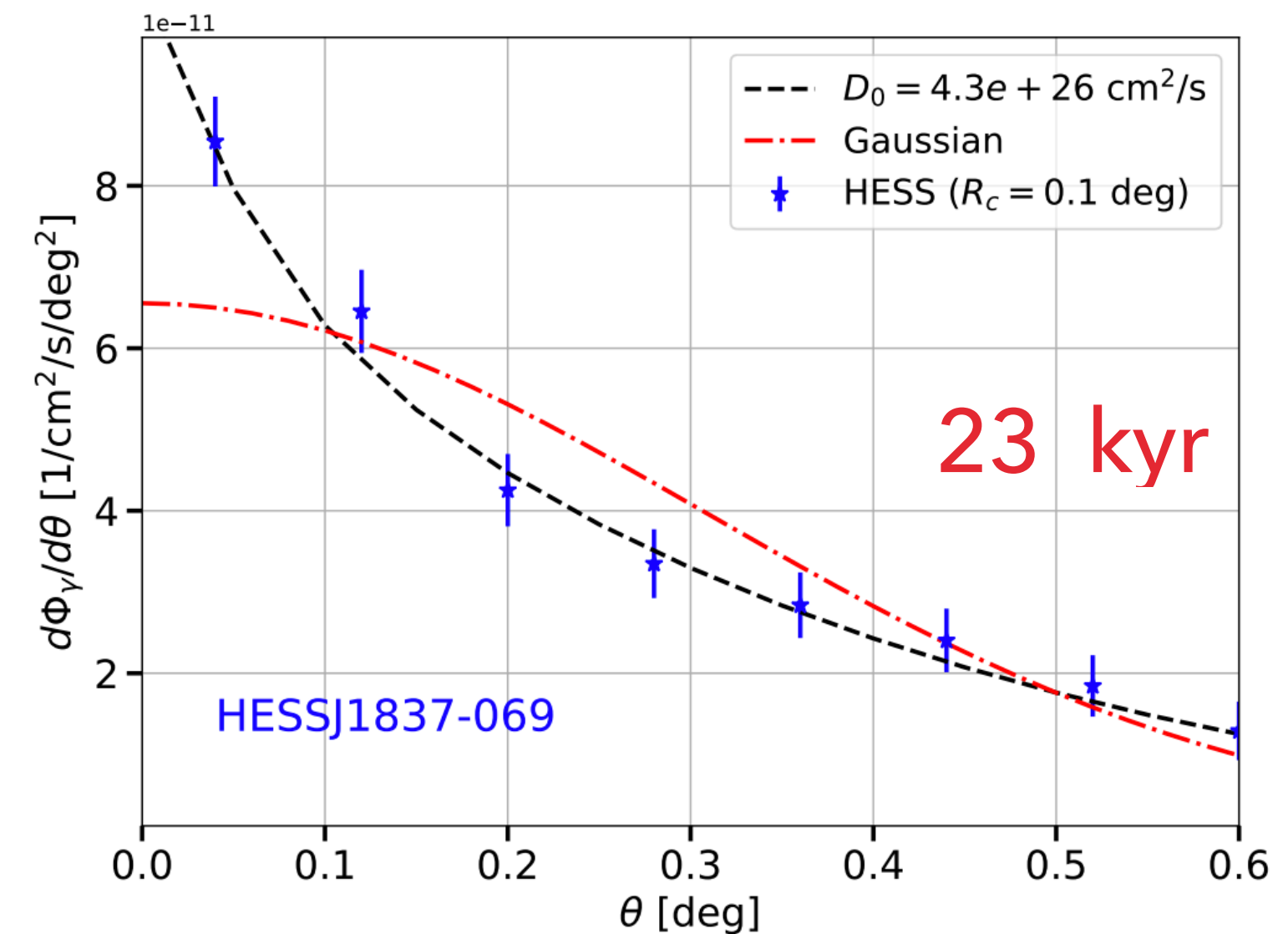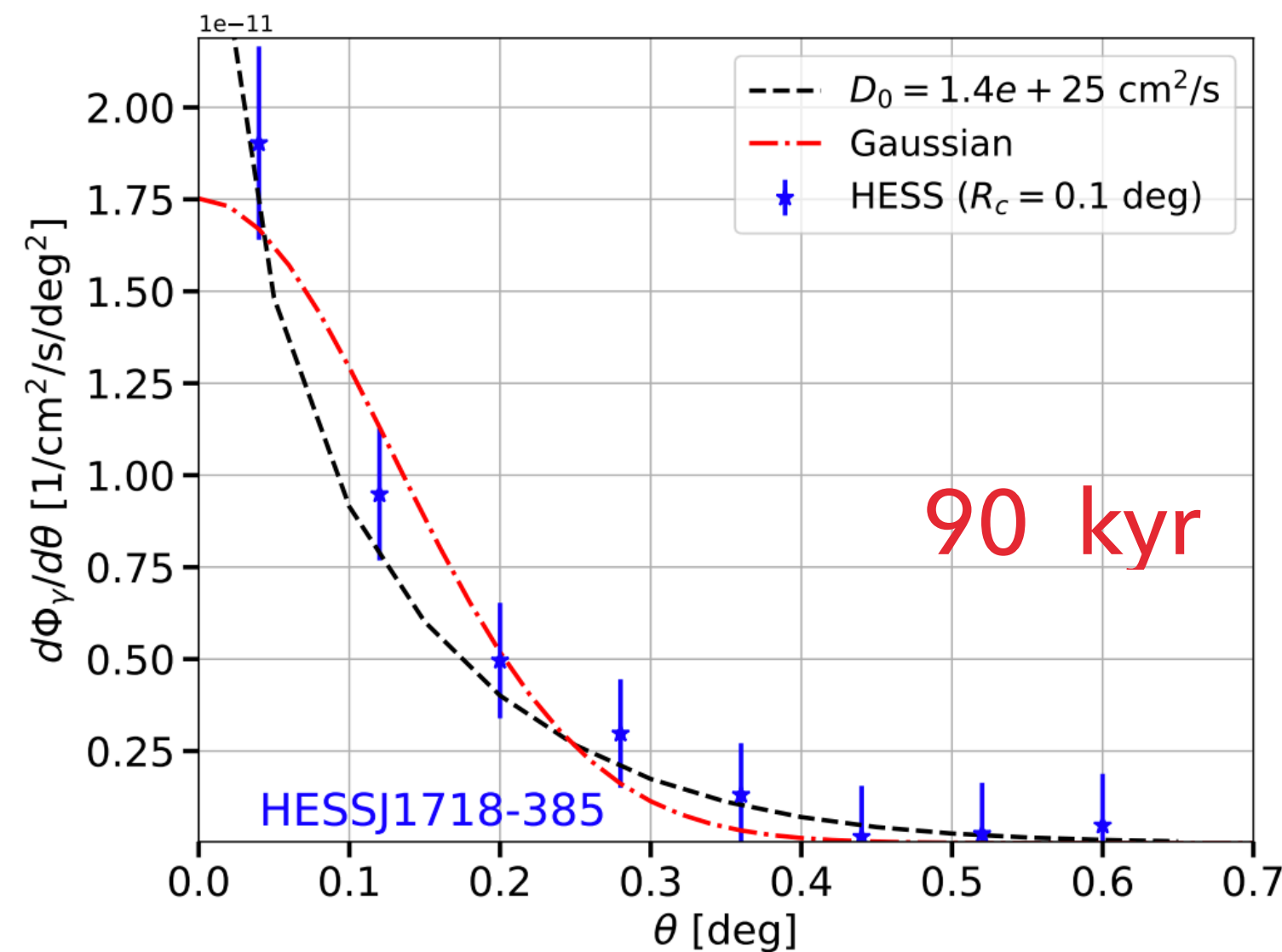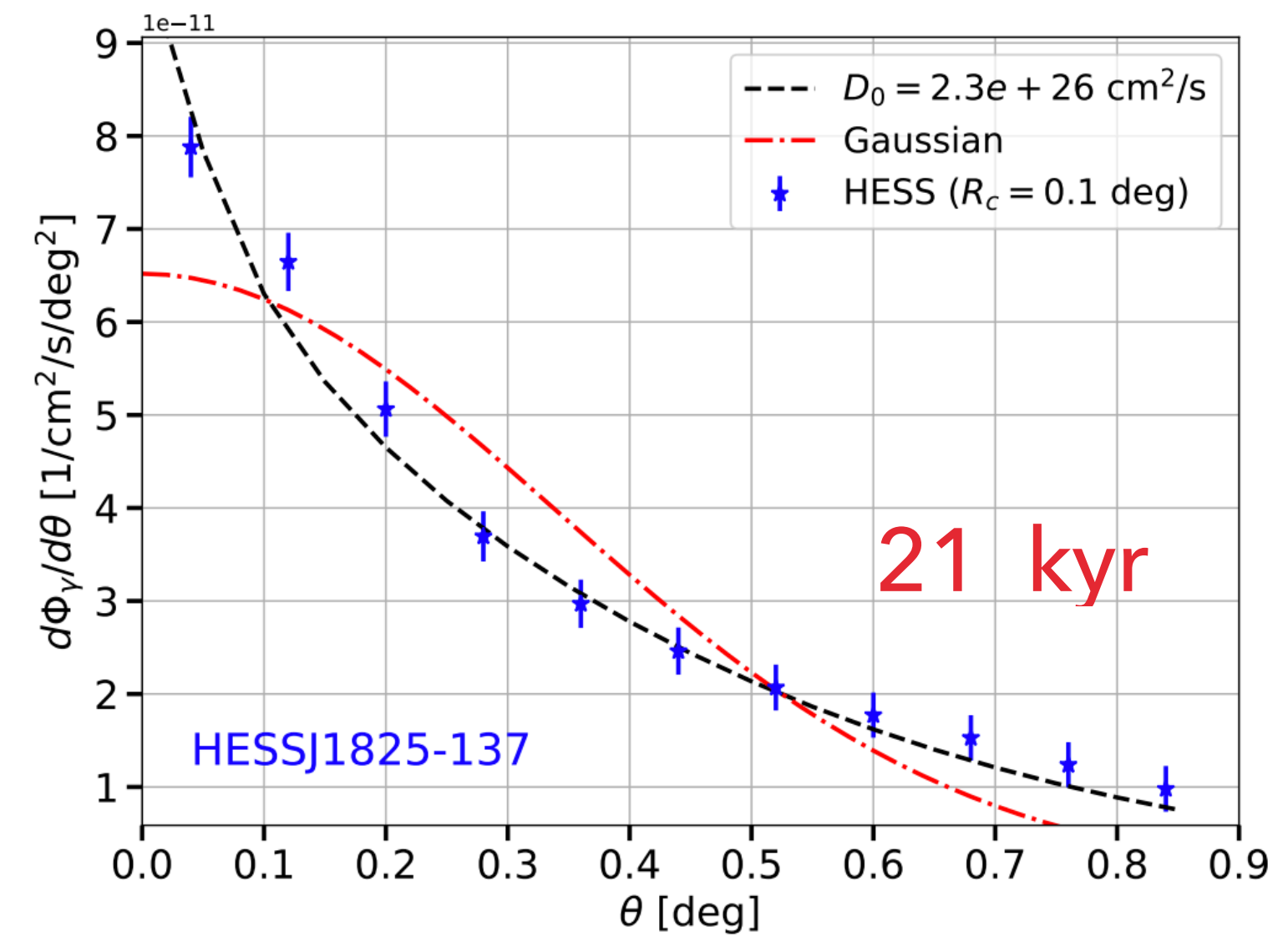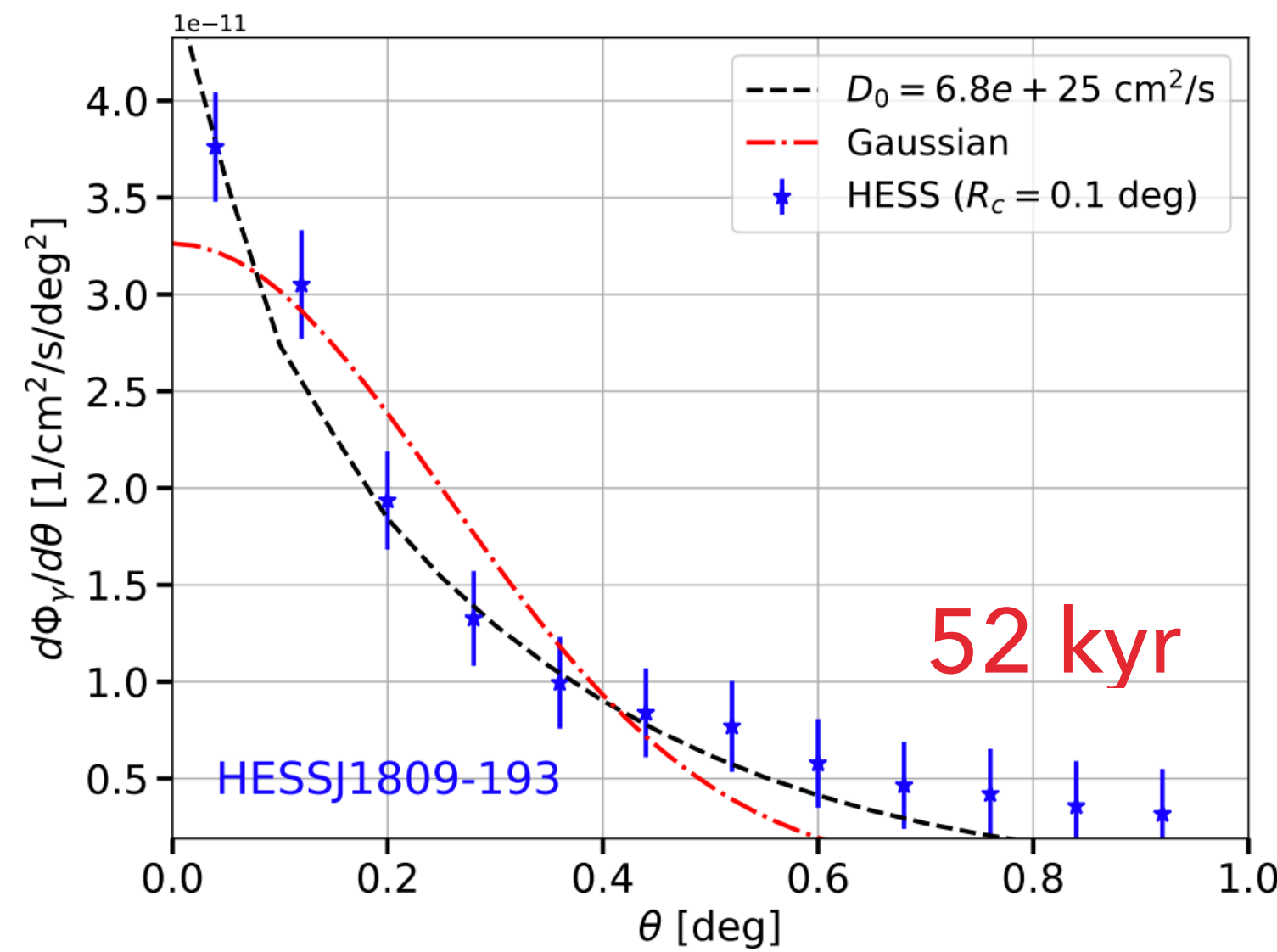
- 8 out of the 9 HAWC sources observed above 56 TeV are consistent with the location of young pulsars.

- Likely PWN or composite objects – but TeV halo contributions must be carefully examined.
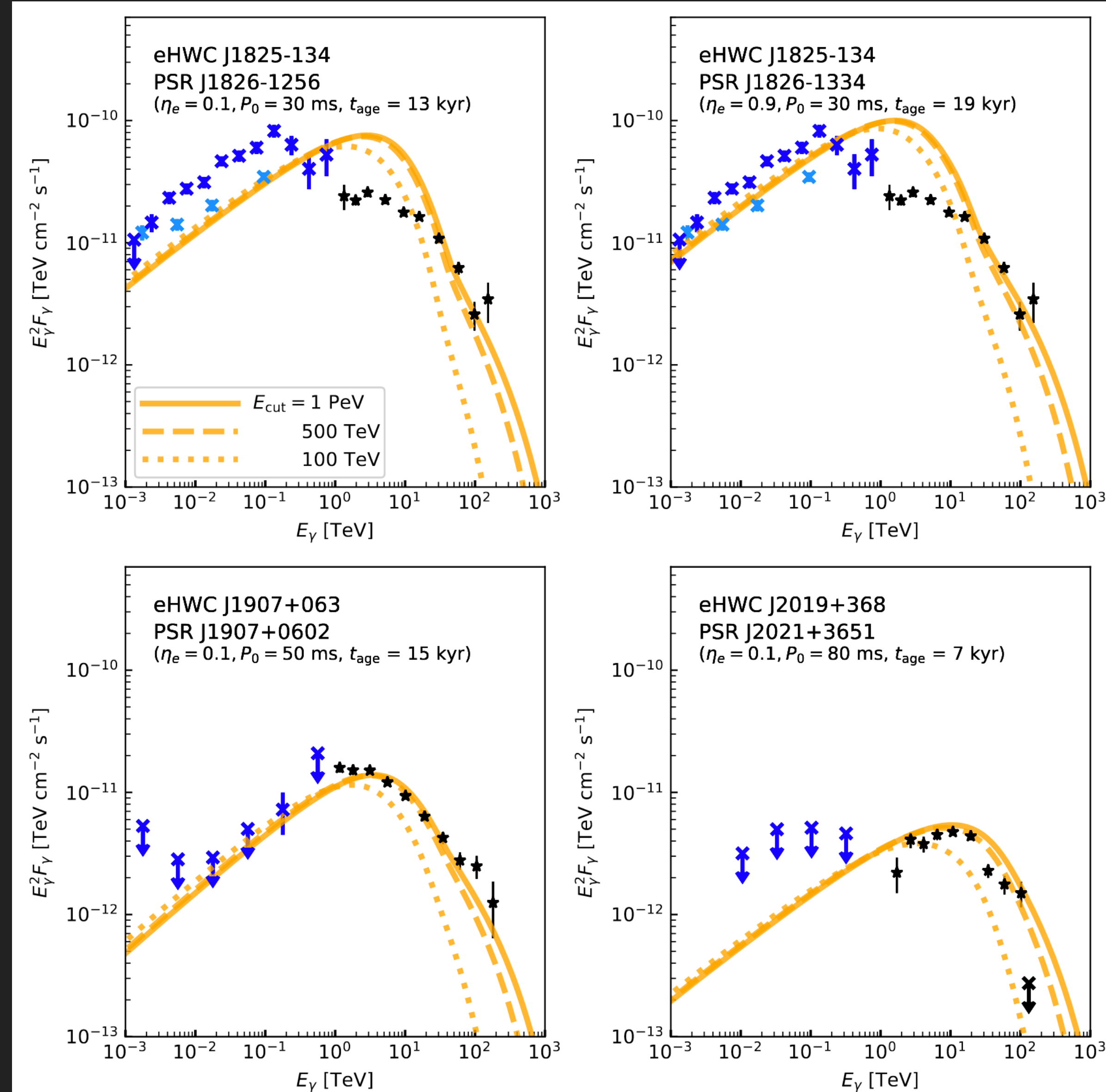
What's in a name? That which we call a rose by any other name would smell as sweet.

William Shakespeare

THE KEY RESULTS - POSITRON EXCESS

- **What were the uncertainties in pulsar models?**

  - **I: The e⁺e⁻ production efficiency?**

    %. A quantitative discussion of plausible values for $f_{e\pm}$ was recently given in Ref. [38]. We shall not review their discussion here, but Ref. [38] argues (see in particular their very informative App. B and C) that in the context of a standard model for the pulsar wind nebulae, a reasonable range for $f_{e\pm}$ falls between 1% and 30%.

  - **II: The e⁺e⁻ spectrum.**

    part of their energy adiabatically because of the expansion of the wind. The energy spectrum injected by a single pulsar depends on the environmental parameters of the pulsar, but some attempts to calculate the average spectrum injected by a population of mature pulsars suggest that the spectrum may be relatively hard, having a slope of ~1.5-1.6 [18]. This spectrum, however, results from a complex interplay of individual pulsar spectra, of the spatial and age distributions of pulsars in the Galaxy, and on the assumption that the chief channel for pulsar spin down is magnetic dipole radiation. Due to the related uncertainties, variations from this injection spectra cannot be ruled out. Typically, one concentrates the attention on pulsars of age ~10^5 years because younger pulsars are likely to still
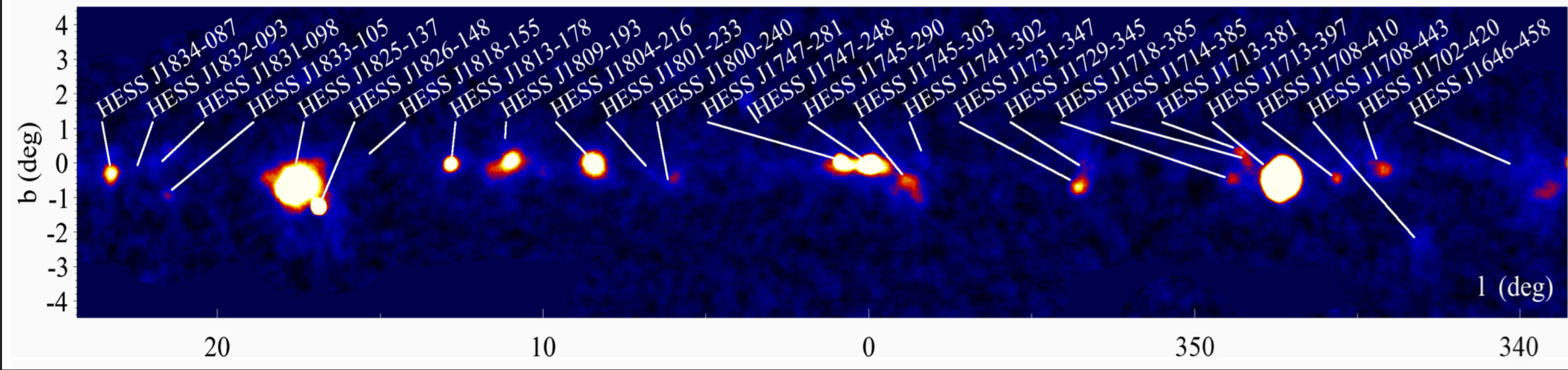
  - **III: The propagation of e⁺e⁻ to Earth.**

    The observed spectrum on Earth of electrons and positrons injected by pulsars is also strongly dependent on propagation effects. In particular, the observed cutoff in the flux of electrons from a pulsar can be much smaller than the injection cutoff due to energy losses ("cooling") during propagation. We define the cooling break, $E_{\mathrm{br}}(t)$, as the maximal energy electrons can have after propagating for time t. Since – as stated above – the typical
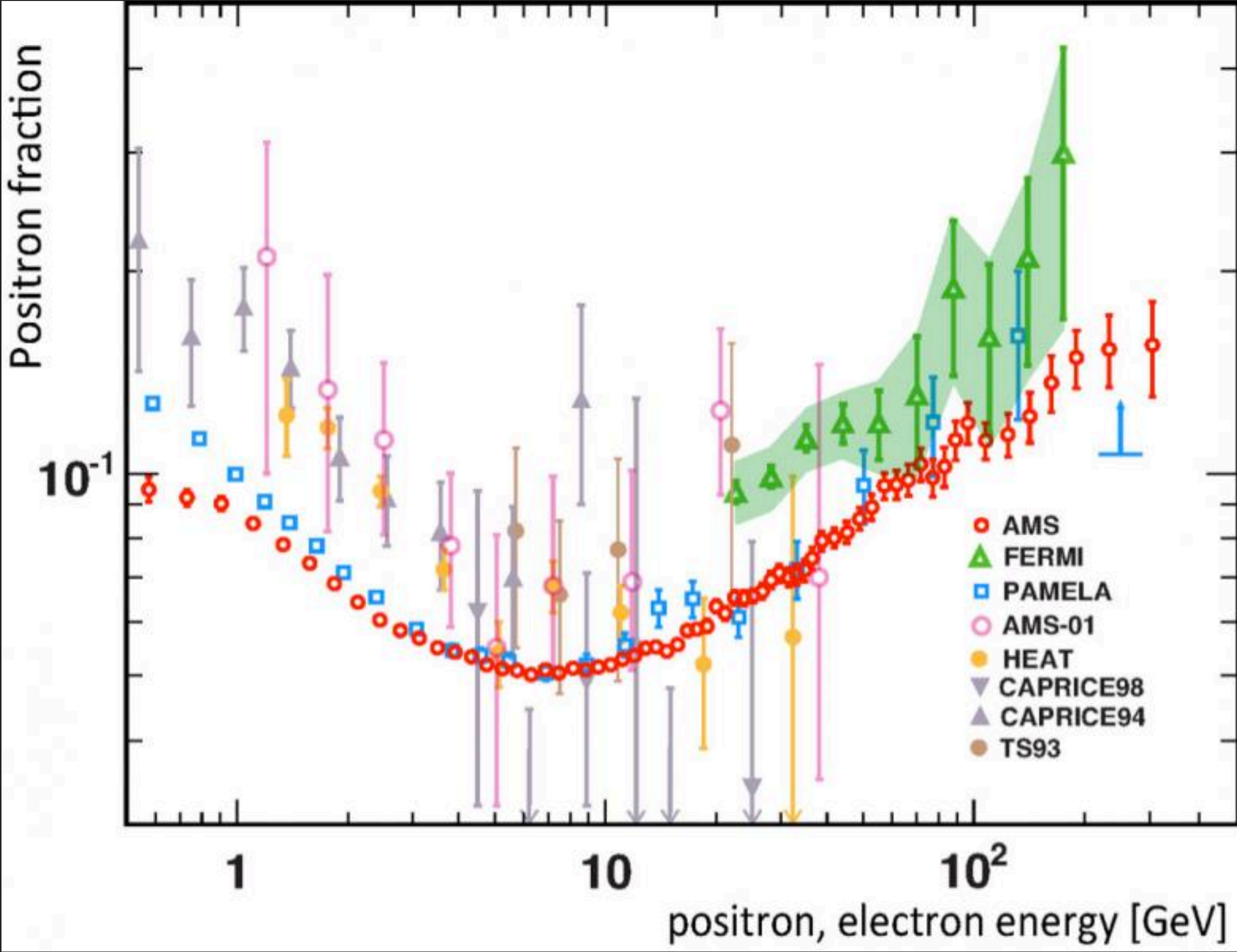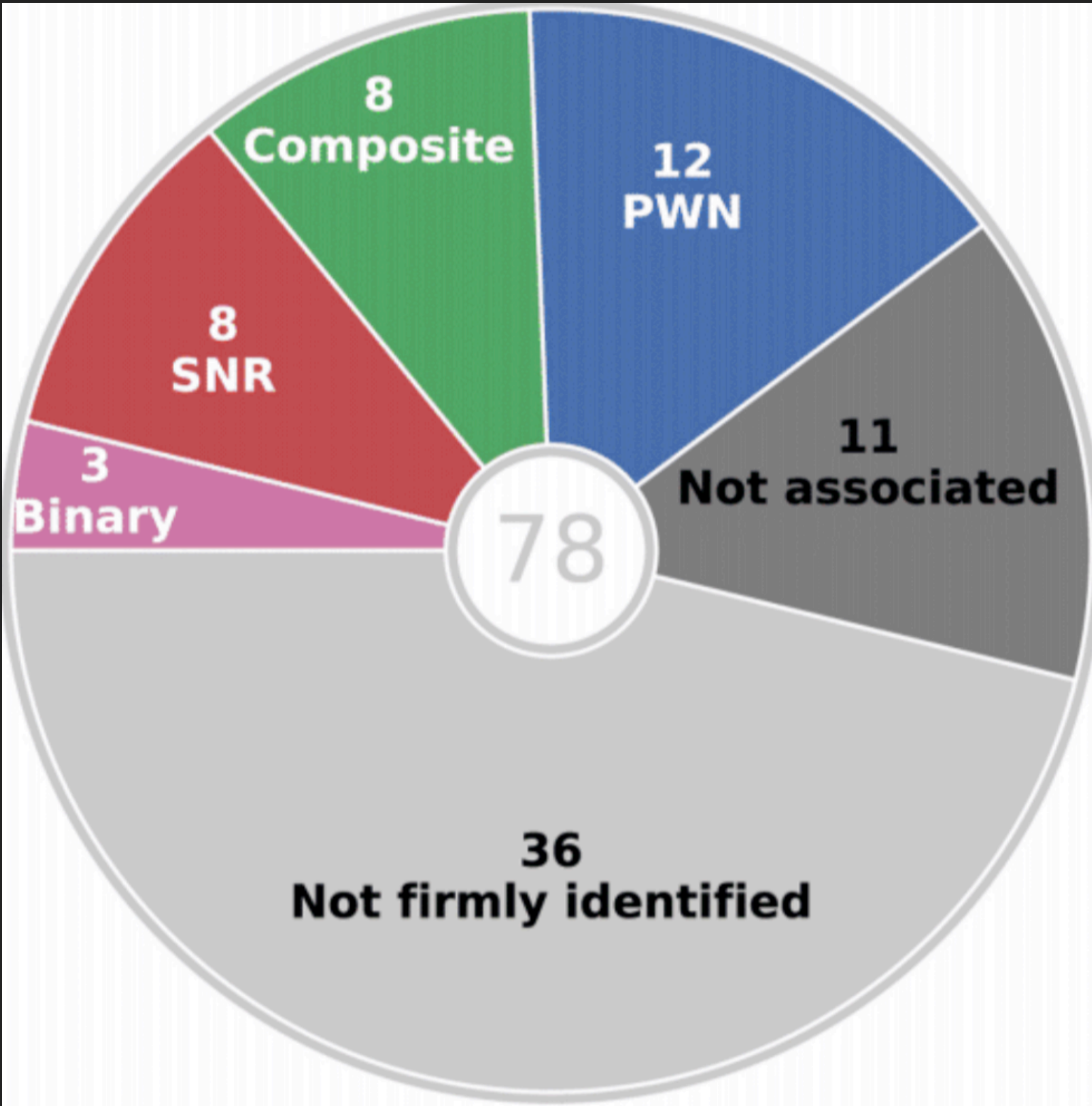
- Radio pulsars are beamed!
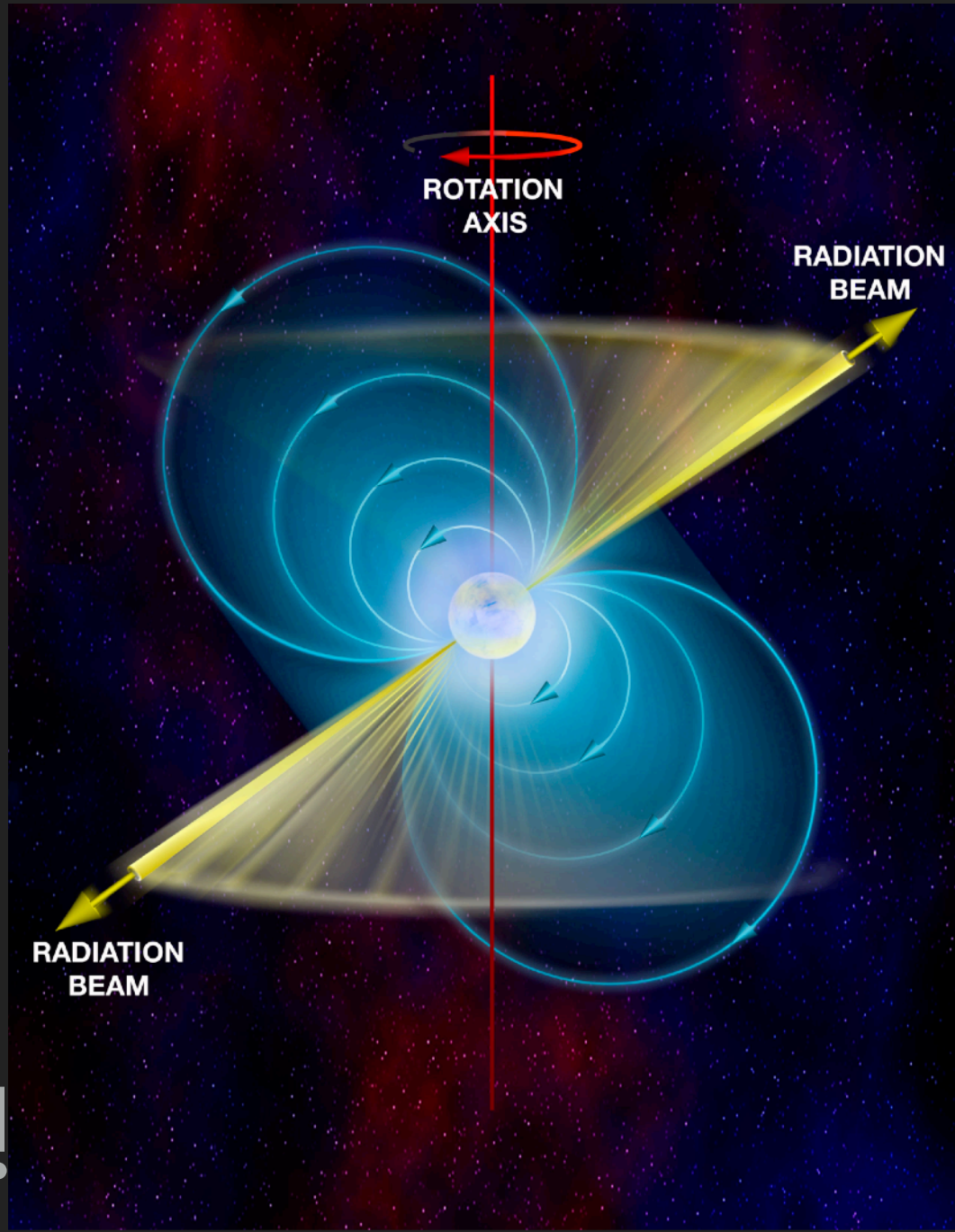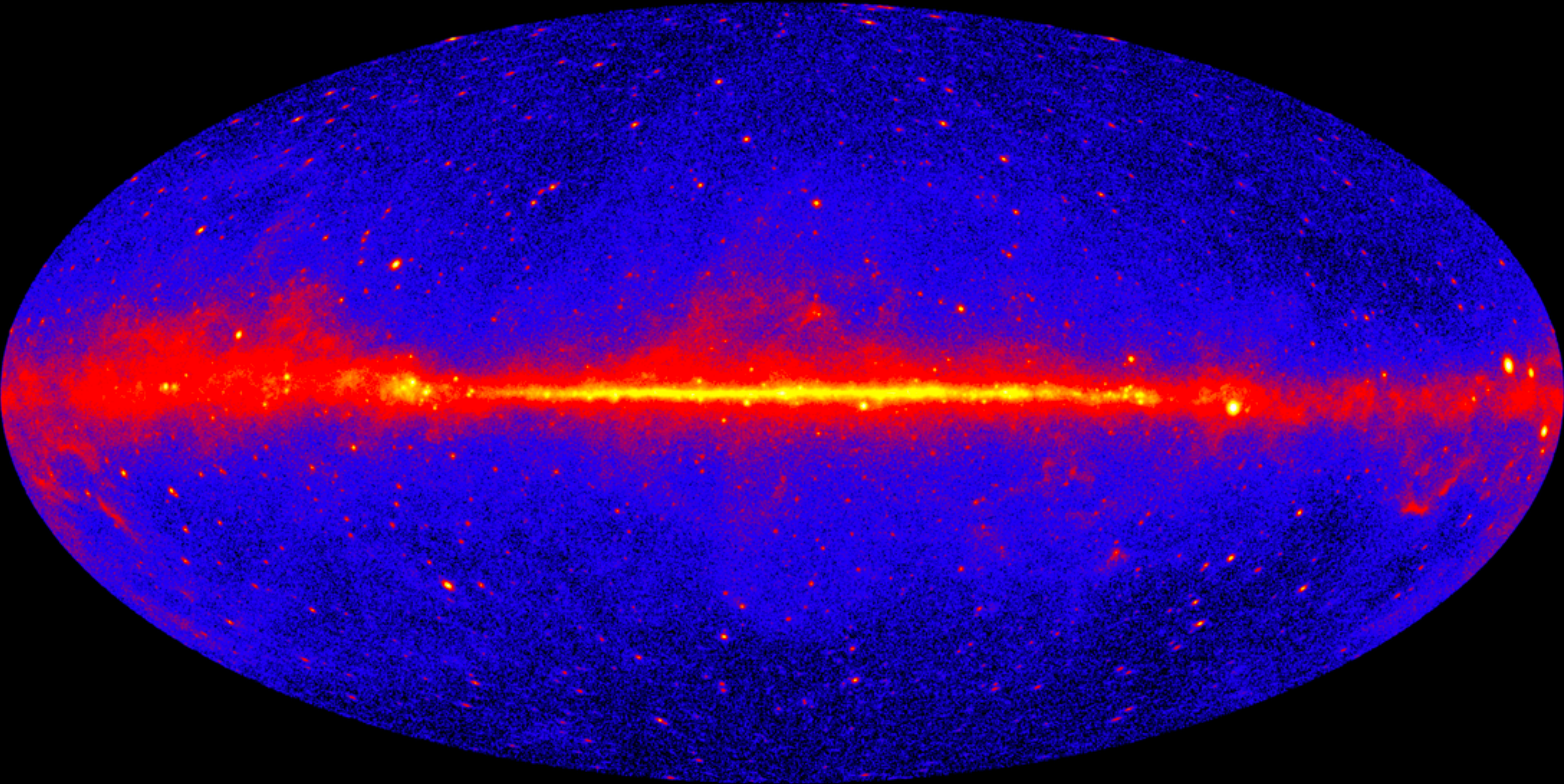

- Beaming fraction is small

Tauris & Manchester (1998)

$$f = \left[1.1 \left(\log_{10} \left(\frac{\tau}{100 \text{ Myr}} \right) \right)^2 + 15 \right] \%$$

- This varies between 15-30%.

- Most pulsars are unseen in radio!
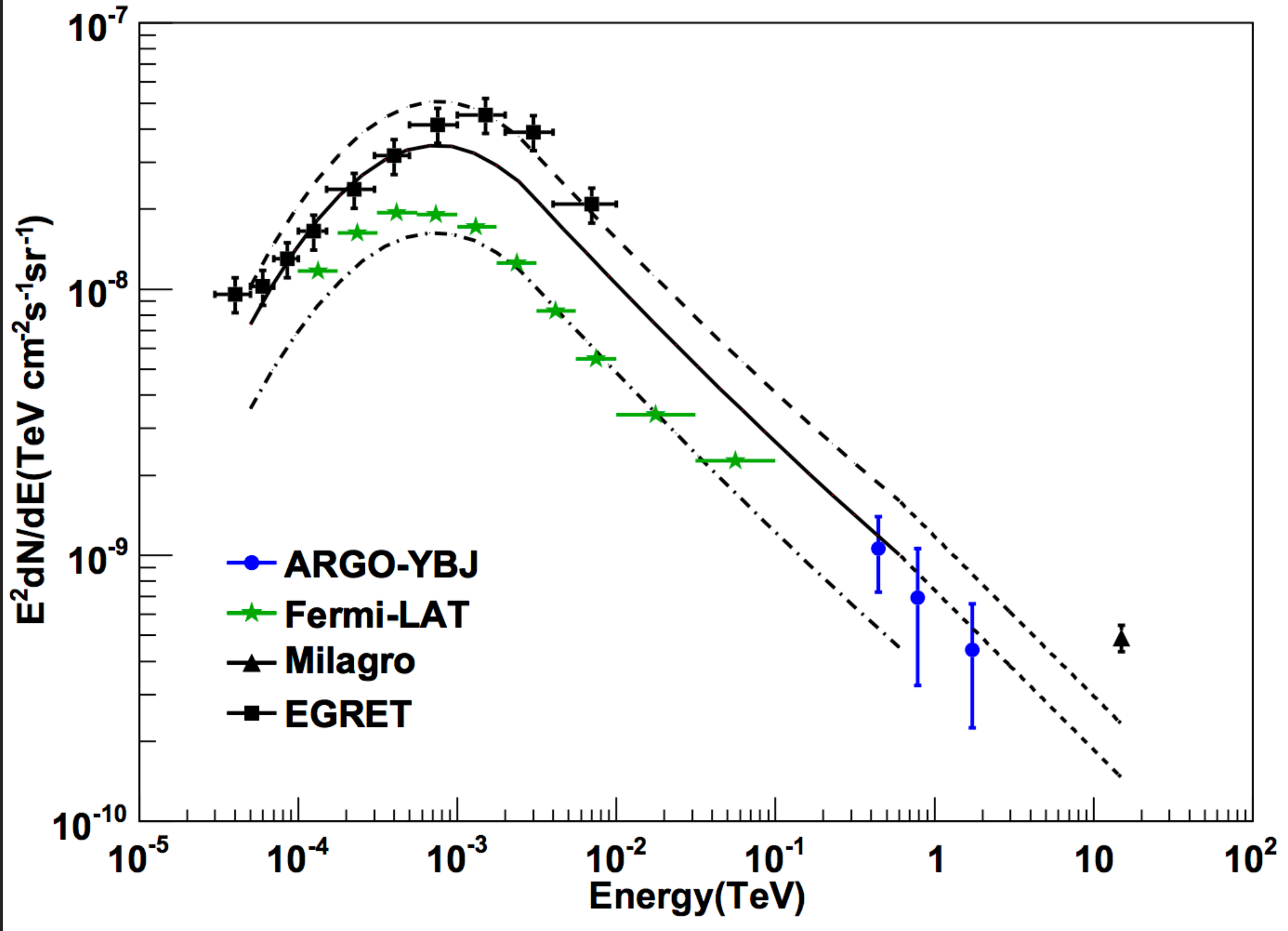
- If TeV halo power is connected to pulsar spin down power, we can build a model of the full TeV sky.


- This means that many young systems should also produce even brighter TeV halo activity!

| #	PSRJ	P0 (s)	P1	DIST (kpc)	AGE (Yr)	BSURF (G)	EDOT (ergs/s)
1	J0537−6910	0.016122	5.18e−14	49.700	4.93e+03	9.25e+11	4.88e+38
2	J0534+2200	0.033392	4.21e−13	2.000	1.26e+03	3.79e+12	4.46e+38
3	J0540−6919	0.050570	4.79e−13	49.700	1.67e+03	4.98e+12	1.46e+38
4	J1813−1749	0.044741	1.27e−13	4.700	5.58e+03	2.41e+12	5.60e+37
5	J1400−6325	0.031182	3.89e−14	7.000	1.27e+04	1.11e+12	5.07e+37
6	J1747−2809	0.052153	1.56e−13	8.141	5.31e+03	2.88e+12	4.33e+37
7	J1833−1034	0.061884	2.02e−13	4.100	4.85e+03	3.58e+12	3.37e+37
8	J2022+3842	0.048579	8.61e−14	10.000	8.94e+03	2.07e+12	2.96e+37
9	J0205+6449	0.065716	1.94e−13	3.200	5.37e+03	3.61e+12	2.70e+37
10	J2229+6114	0.051624	7.83e−14	3.000	1.05e+04	2.03e+12	2.25e+37
11	J1513−5908	0.151582	1.53e−12	4.400	1.57e+03	1.54e+13	1.73e+37
12	J1617−5055	0.069357	1.35e−13	4.743	8.13e+03	3.10e+12	1.60e+37
13	J1124−5916	0.135477	7.53e−13	5.000	2.85e+03	1.02e+13	1.19e+37
14	J1930+1852	0.136855	7.51e−13	7.000	2.89e+03	1.03e+13	1.16e+37
15	J1023−5746	0.111472	3.84e−13	2.080	4.60e+03	6.62e+12	1.09e+37
16	J1420−6048	0.068180	8.32e−14	5.632	1.30e+04	2.41e+12	1.04e+37
17	J1410−6132	0.050052	3.20e−14	13.510	2.48e+04	1.28e+12	1.01e+37
18	J1849−0001	0.038523	1.42e−14	*	4.31e+04	7.47e+11	9.78e+36
19	J1402+13	0.005890	4.83e−17	*	1.93e+06	1.71e+10	9.34e+36
20	J1846−0258	0.326571	7.11e−12	5.800	7.28e+02	4.88e+13	8.06e+36
21	J0835−4510	0.089328	1.25e−13	0.280	1.13e+04	3.38e+12	6.92e+36
22	J1811−1925	0.064667	4.40e−14	5.000	2.33e+04	1.71e+12	6.42e+36
23	J1111−6039	0.106670	1.95e−13	*	8.66e+03	4.62e+12	6.35e+36
24	J1813−1246	0.048072	1.76e−14	2.635	4.34e+04	9.30e+11	6.24e+36
25	J1838−0537	0.145708	4.72e−13	*	4.89e+03	8.39e+12	6.02e+36
26	J1838−0655	0.070498	4.92e−14	6.600	2.27e+04	1.89e+12	5.55e+36
27	J1418−6058	0.110573	1.69e−13	1.885	1.03e+04	4.38e+12	4.95e+36
28	J1935+2025	0.080118	6.08e−14	4.598	2.09e+04	2.23e+12	4.66e+36
29	J1856+0245	0.080907	6.21e−14	6.318	2.06e+04	2.27e+12	4.63e+36
30	J1112−6103	0.064962	3.15e−14	4.500	3.27e+04	1.45e+12	4.53e+36
31	J1640−4631	0.206443	9.76e−13	12.750	3.35e+03	1.44e+13	4.38e+36
32	J1844−0346	0.112855	1.55e−13	*	1.16e+04	4.23e+12	4.25e+36
33	J1952+3252	0.039531	5.84e−15	3.000	1.07e+05	4.86e+11	3.74e+36
34	J1826−1256	0.110224	1.21e−13	1.550	1.44e+04	3.70e+12	3.58e+36
35	J1709−4429	0.102459	9.30e−14	2.600	1.75e+04	3.12e+12	3.41e+36
36	J2021+3651	0.103741	9.57e−14	1.800	1.72e+04	3.19e+12	3.38e+36
37	J1524−5625	0.078219	3.90e−14	3.378	3.18e+04	1.77e+12	3.21e+36
38	J1357−6429	0.166108	3.60e−13	3.100	7.31e+03	7.83e+12	3.10e+36
39	J1913+1011	0.035909	3.37e−15	4.613	1.69e+05	3.52e+11	2.87e+36
40	J1826−1334	0.101487	7.53e−14	3.606	2.14e+04	2.80e+12	2.84e+36

Linden & Buckman (2017; 1707.01905)

- If all convert a similar fraction of their spin down power to e+e- pairs as Geminga, then TeV halos naturally explain this observation.

- Note - "Halo" is not needed
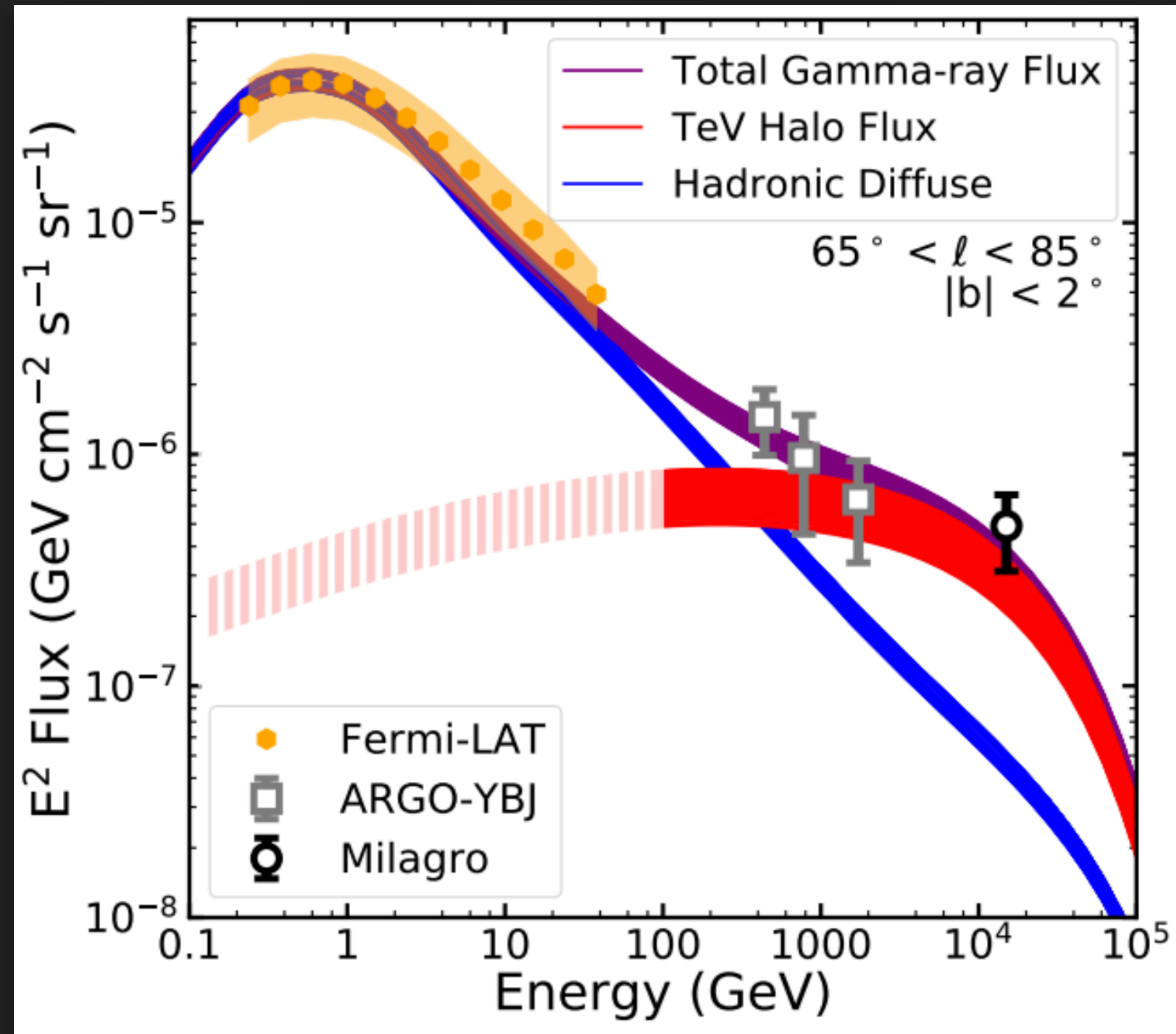
  - Pulsar efficiency ~10%
  - Power must escape PWN

- TeV halos naturally explain the spectrum and intensity of this emission.

- Multiple halos observed with E$^{-2.0}$ spectra.

- Note - "Halo" is not needed
  - Pulsar efficiency ~10%
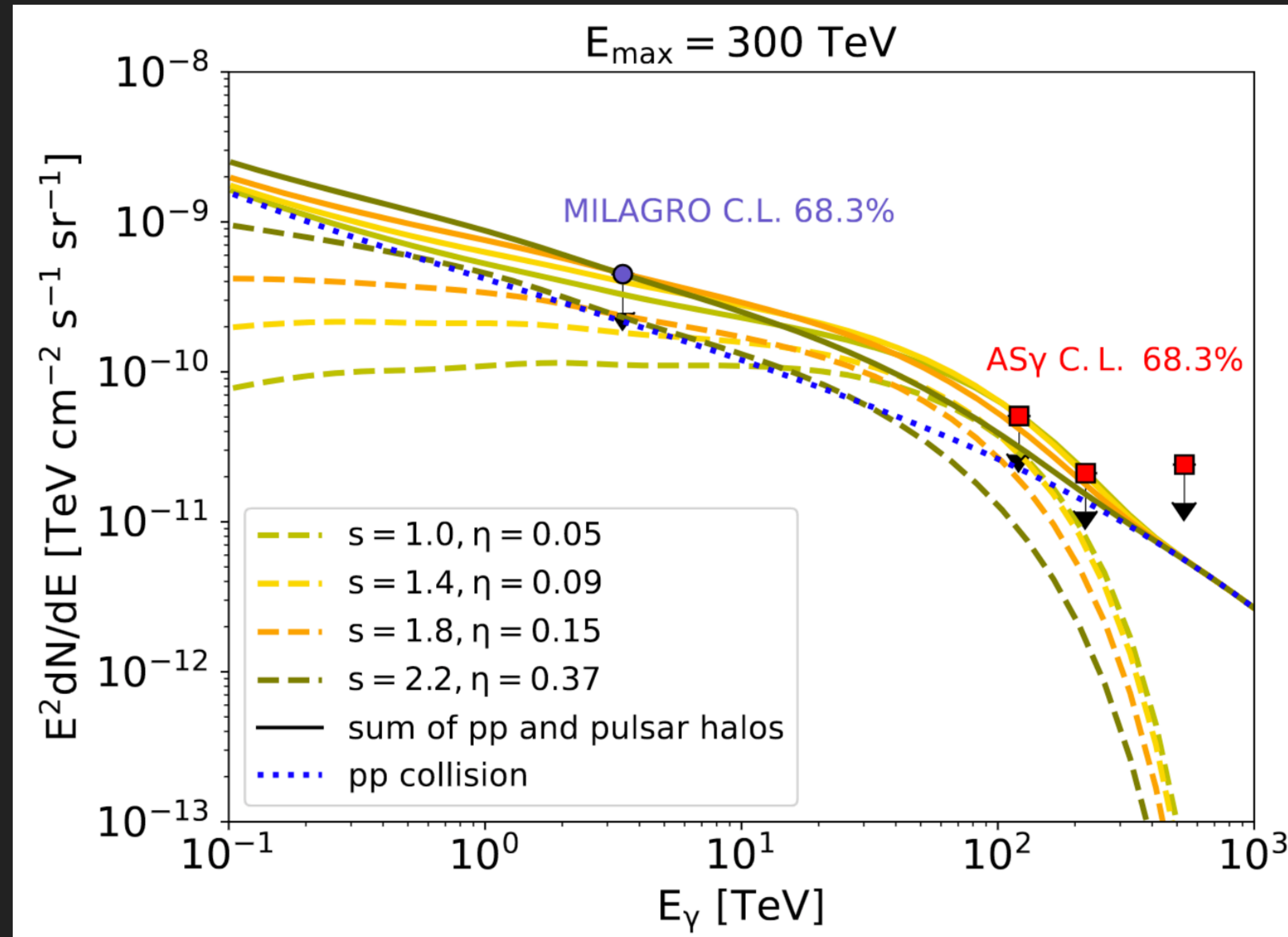 - Power must escape PWN

Fang & Murase (2021; 2104.09491)
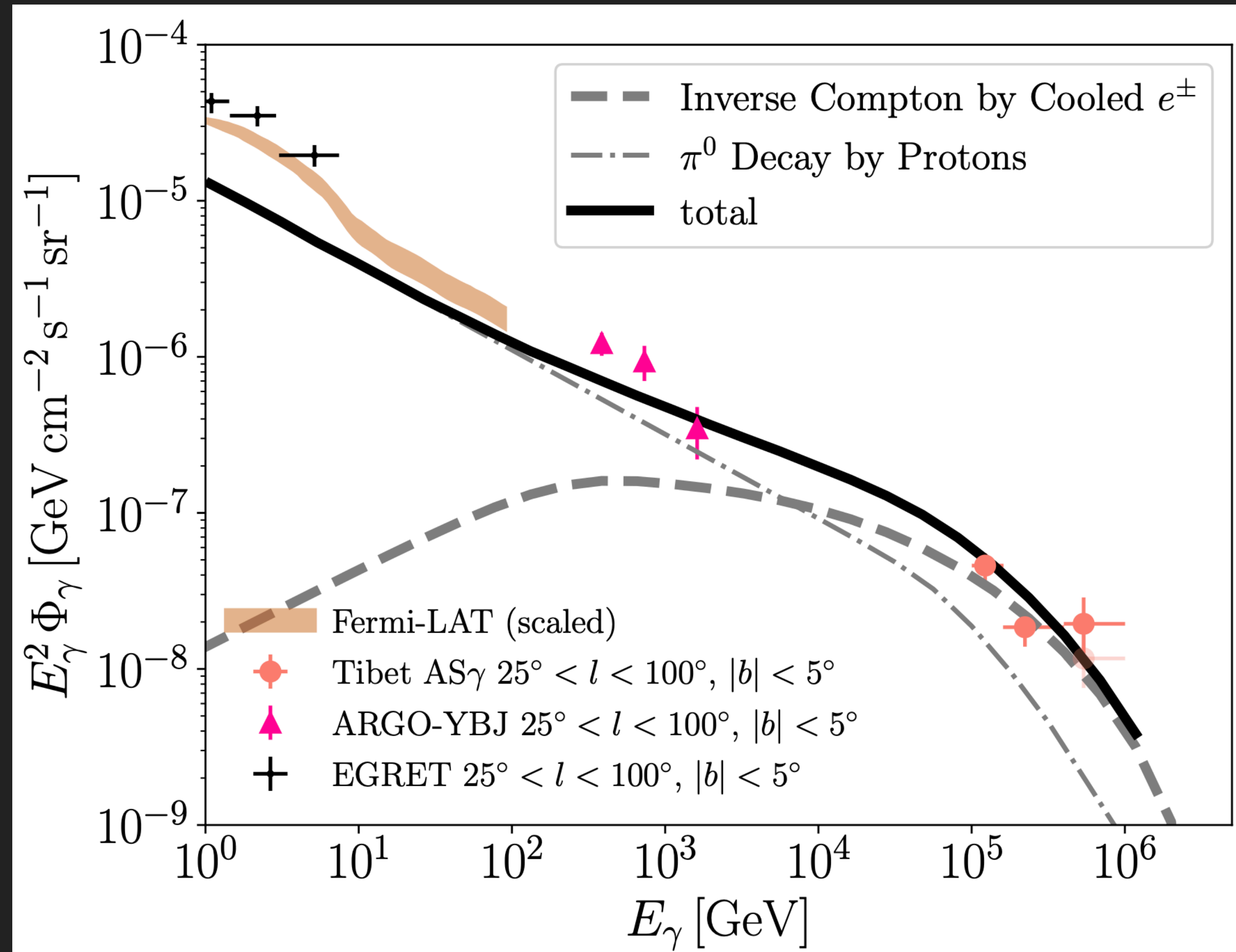
Tibet ASγ data

- TeV halos naturally explain the spectrum and intensity of this emission.

- Multiple halos observed with E$^{-2.0}$ spectra.

- Note - "Halo" is not needed
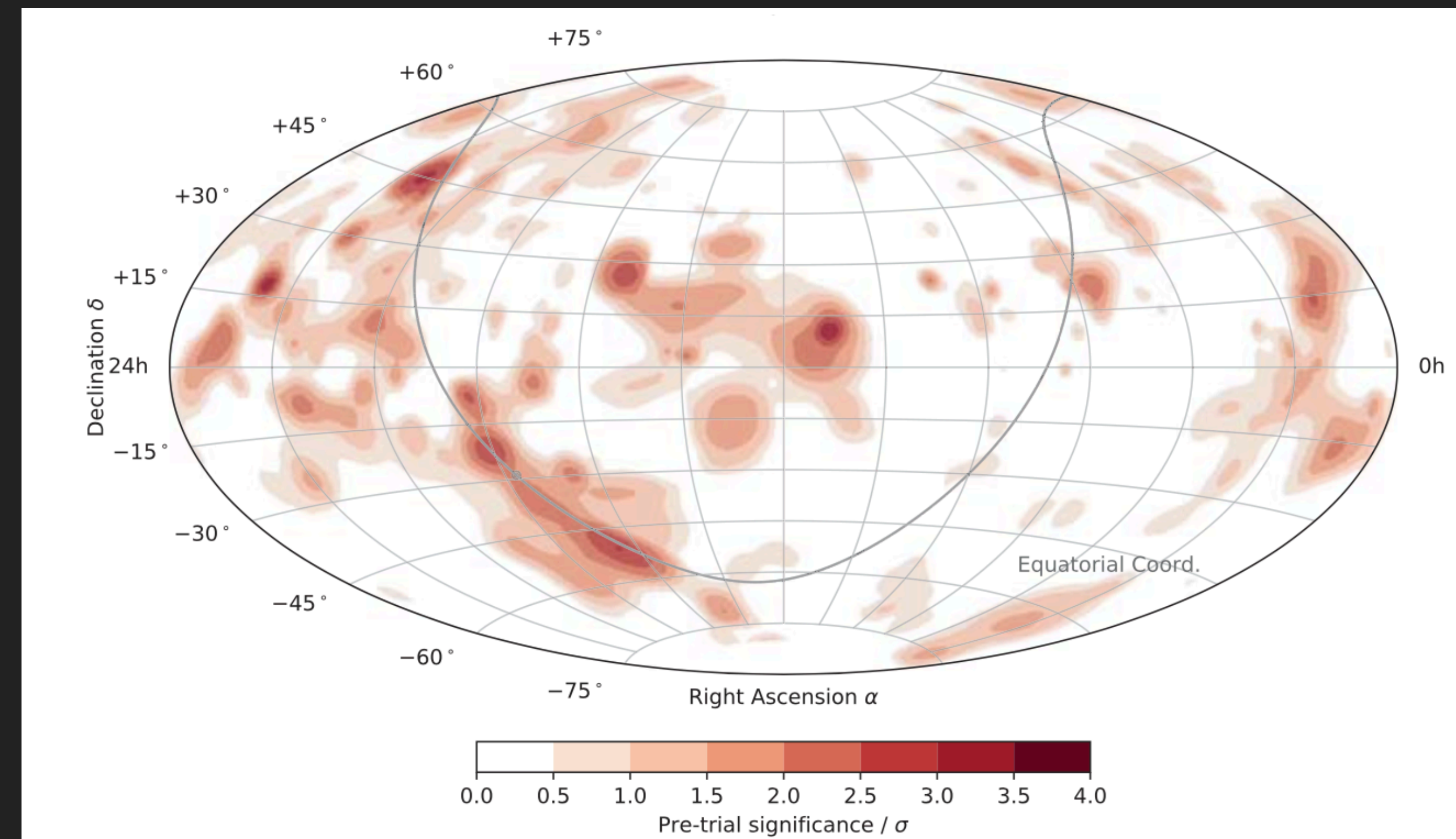 - Pulsar efficiency ~10%
 - Power must escape PWN

Yan & Liu (2023; 2304.12574)

LHAASO Data

▸ IceCube detection of a galactic neutrino flux – with a normalization that is ~4x brighter than expectations from the Fermi-LAT extrapolation.
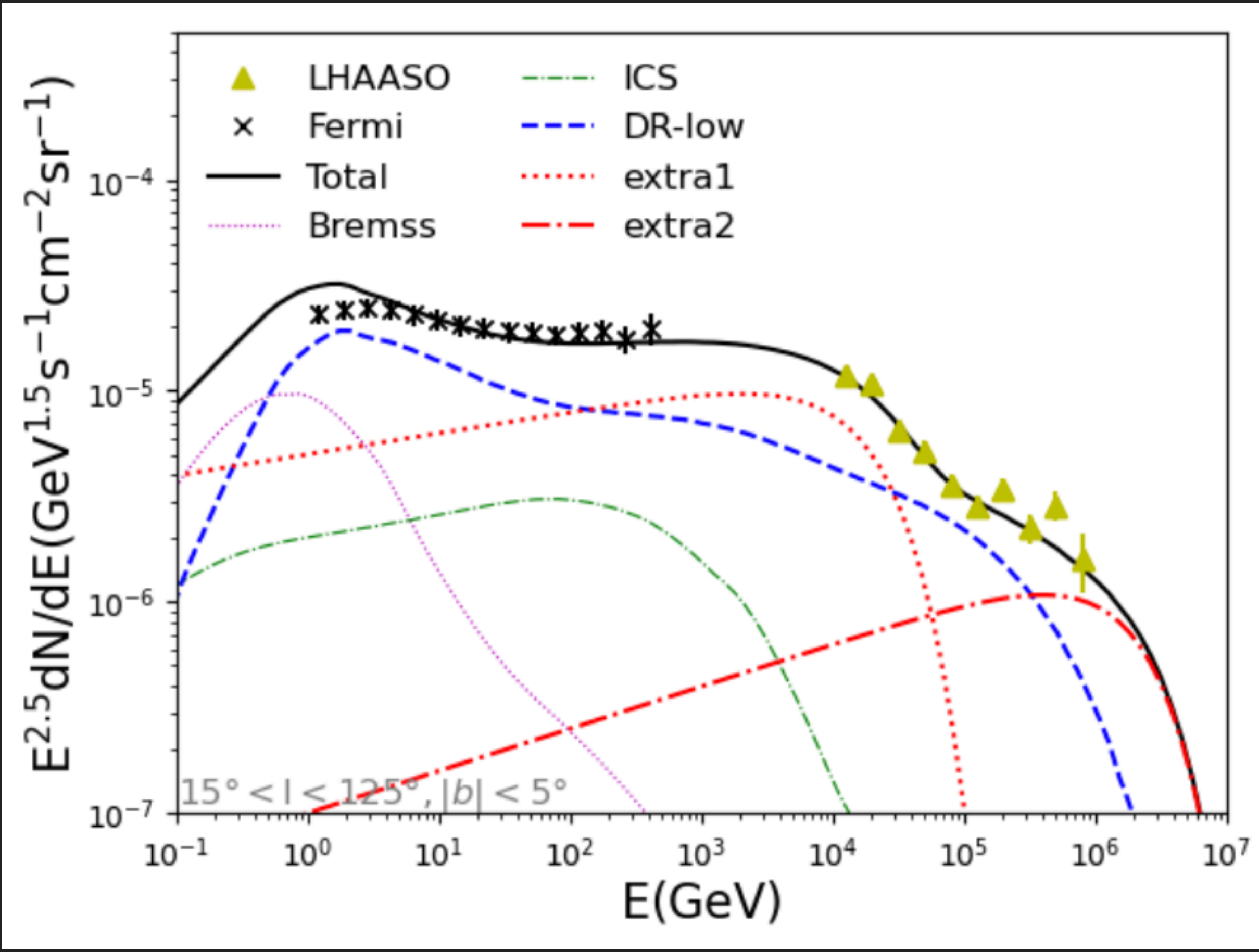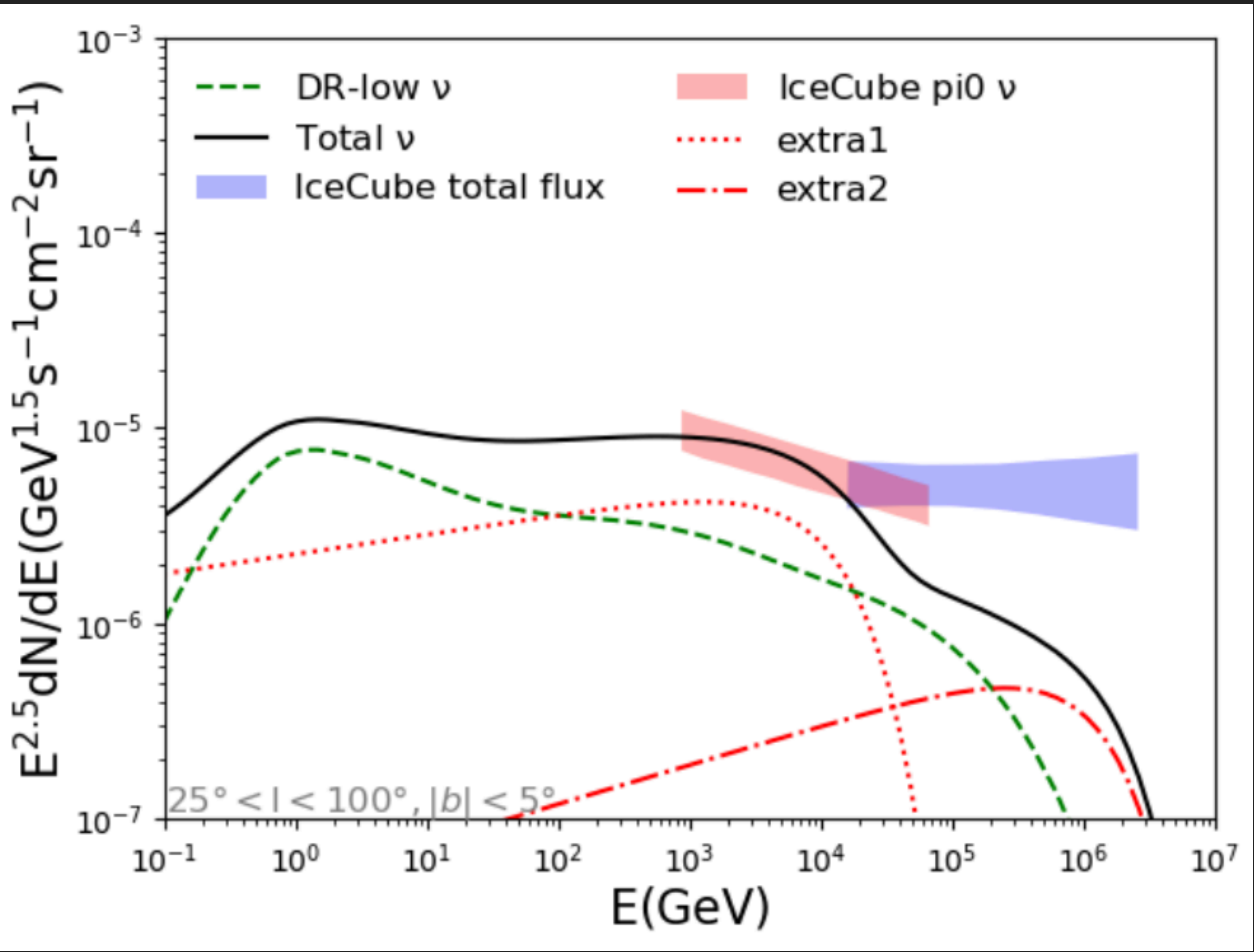
- If the IceCube neutrino flux from the galaxy is higher, then the gamma-ray flux from hadronic processes (i.e., not halos) could also be higher.

- In Fang et al. this is capable of producing the diffuse galactic gamma-ray emission
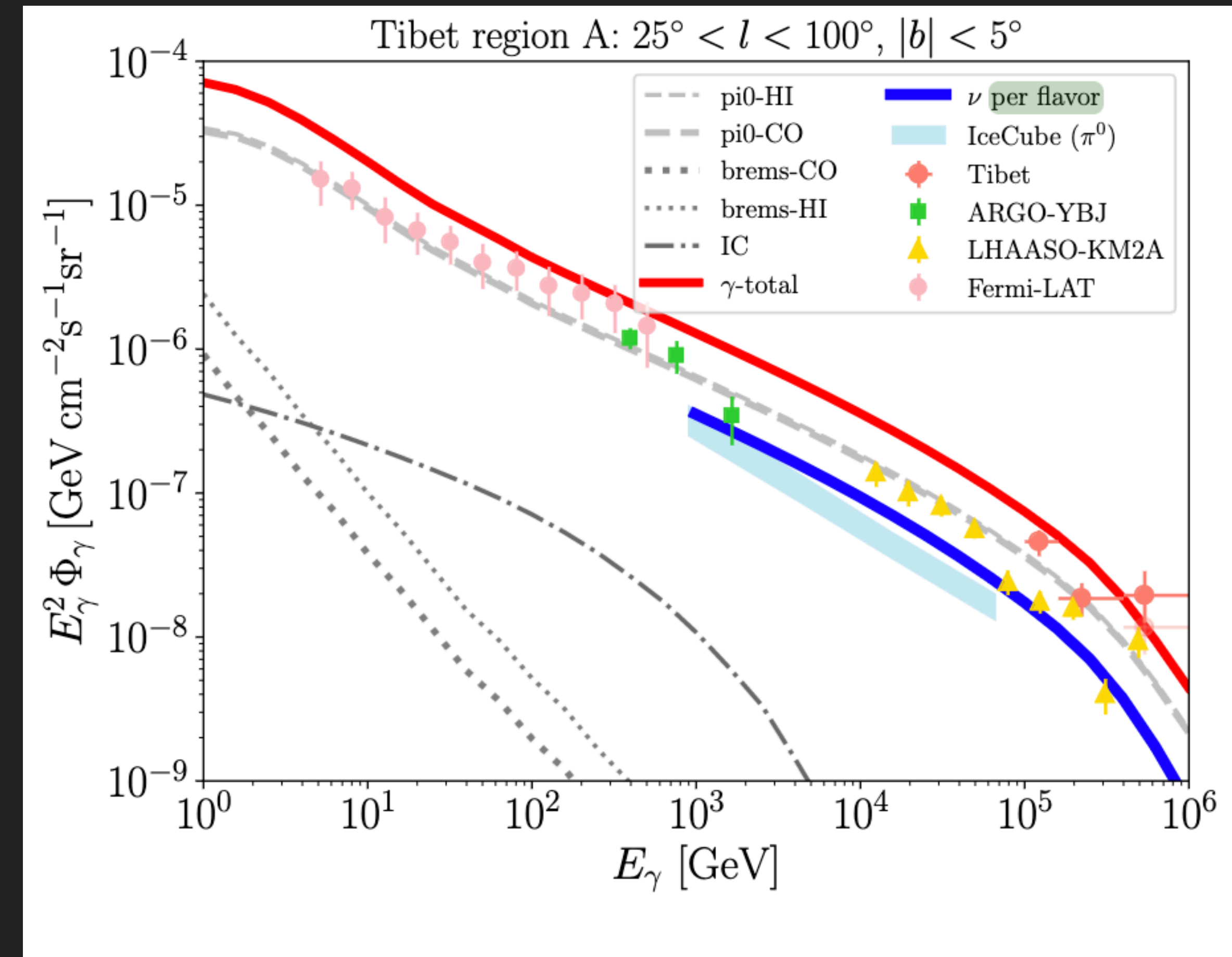
- Models that explain the IceCube neutrino flux still require an additional gamma-ray component (here: "Extra1 and Extra2") to produce the gamma-ray data from LHAASO.

MANY CAVEATS

- IceCube neutrino flux is unknown at low energies (nearly order of magnitude uncertainties from models that fit the data to within 1σ.

- On top of this, there is an intrinsic factor of 2 uncertainty in even the IceCube flux measurement.

- There is also a factor of ~2 uncertainty in the TeV halo flux owing to the "Geminga-like" assumption
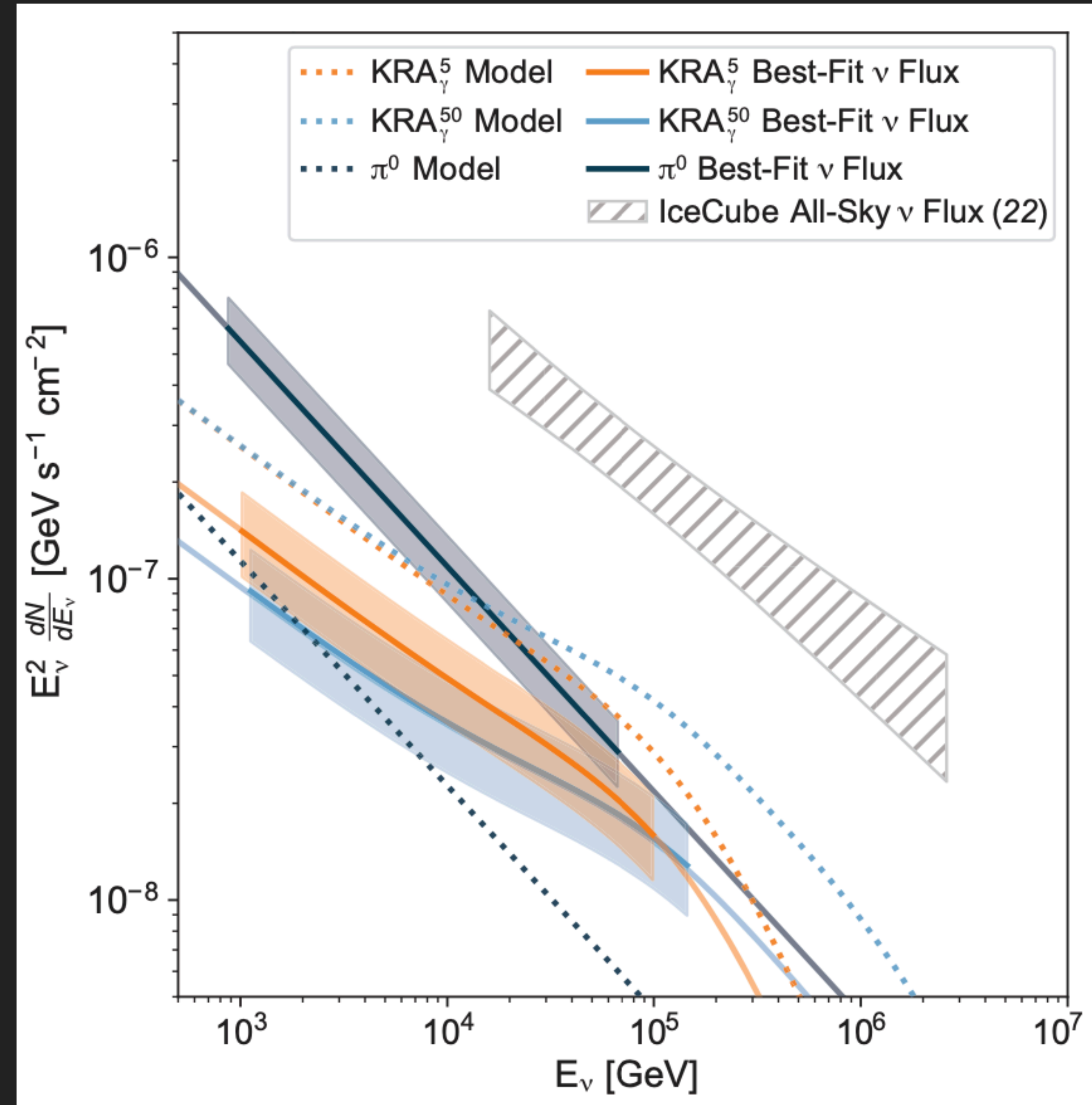
TEV HALOS BREAK STANDARD DIFFUSE MODELS
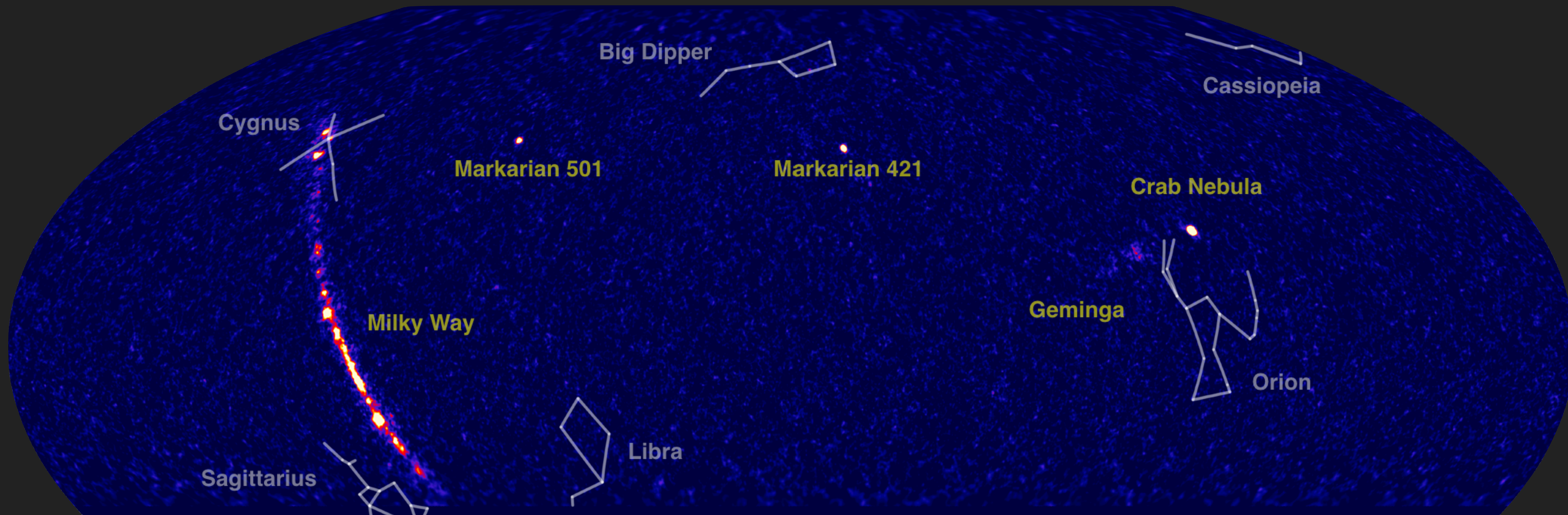
- There is bright diffuse gamma-ray emission across the galactic plane.

- Ratio of point source emission to diffuse emission is a powerful marker of emission mechanisms and local propagation.

- High Angular Resolution

- Long energy-lever arm (20 GeV – 100 TeV)

- Bifurcation in electron/proton morphology
  - $D_{\mathrm{proton}} \propto E^{\delta/2}$
  - $D_{\mathrm{electron}} \propto E^{\delta/2-1}$

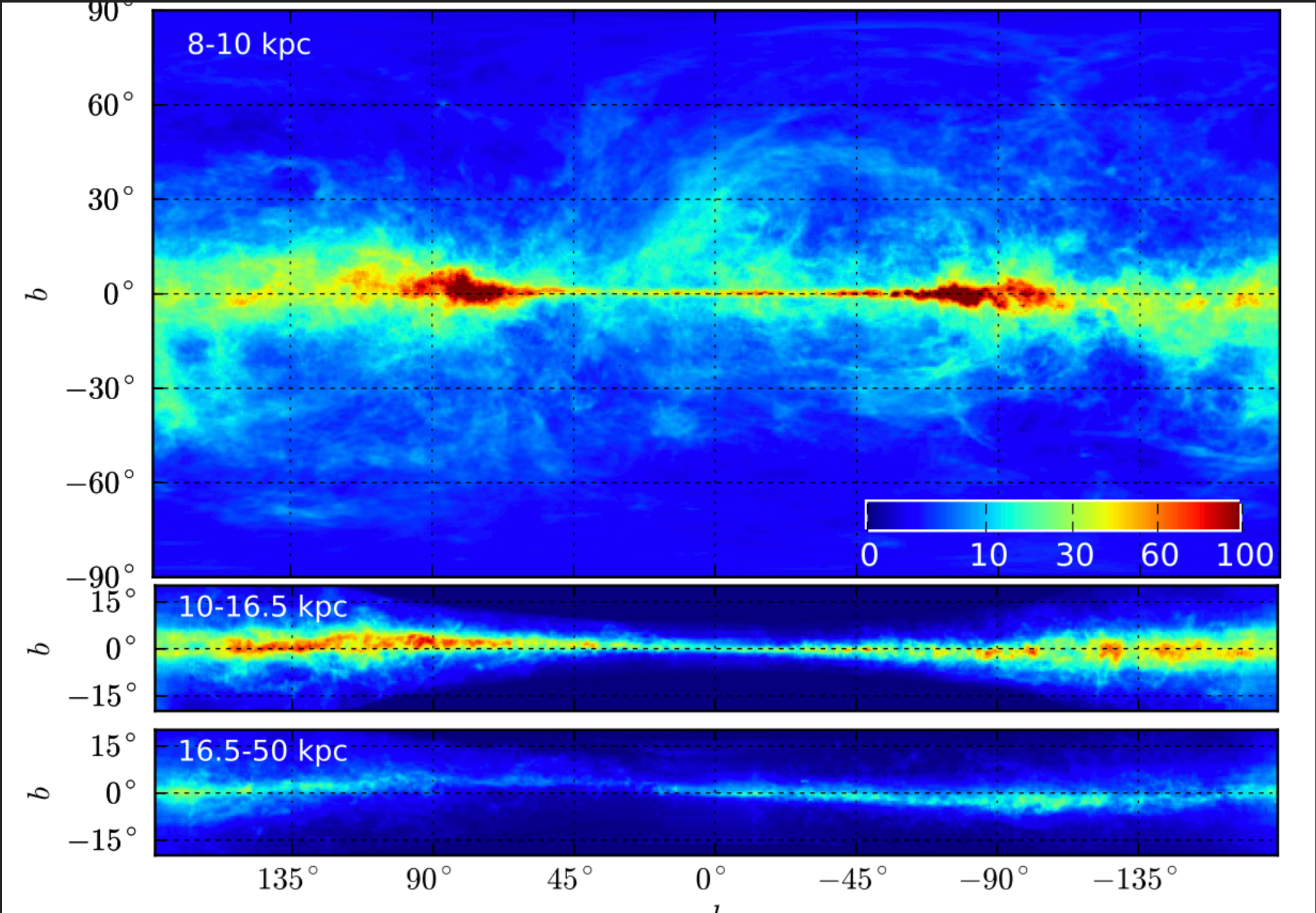$$\underbrace{\frac{\partial \psi(\vec{r},p,t)}{\partial t}}_{\text{flux}} = \underbrace{Q(\vec{r},p,t)}_{\text{source}} + \vec{\nabla} \times (\ \underbrace{D_{xx}\vec{\nabla}\psi}_{\text{diffusion}} \ - \ \underbrace{\vec{V}\psi}_{\text{convection}}\ ) + \overbrace{\underbrace{\frac{\partial}{\partial p}p^2 D_{pp}\frac{\partial}{\partial p^2}\psi}_{}}^{\text{re-acceleration}}$$

$$\underbrace{-\frac{\partial}{\partial p}\left(\dot{p}\psi - \frac{p}{3}\left(\vec{\nabla}\times\vec{V}\right)\psi\right)}_{\text{energy loss}} \ - \ \underbrace{\frac{\psi}{\tau_f}}_{\text{fragmentation}} \ - \ \underbrace{\frac{\psi}{\tau_r}}_{\text{radioactive decay}}$$
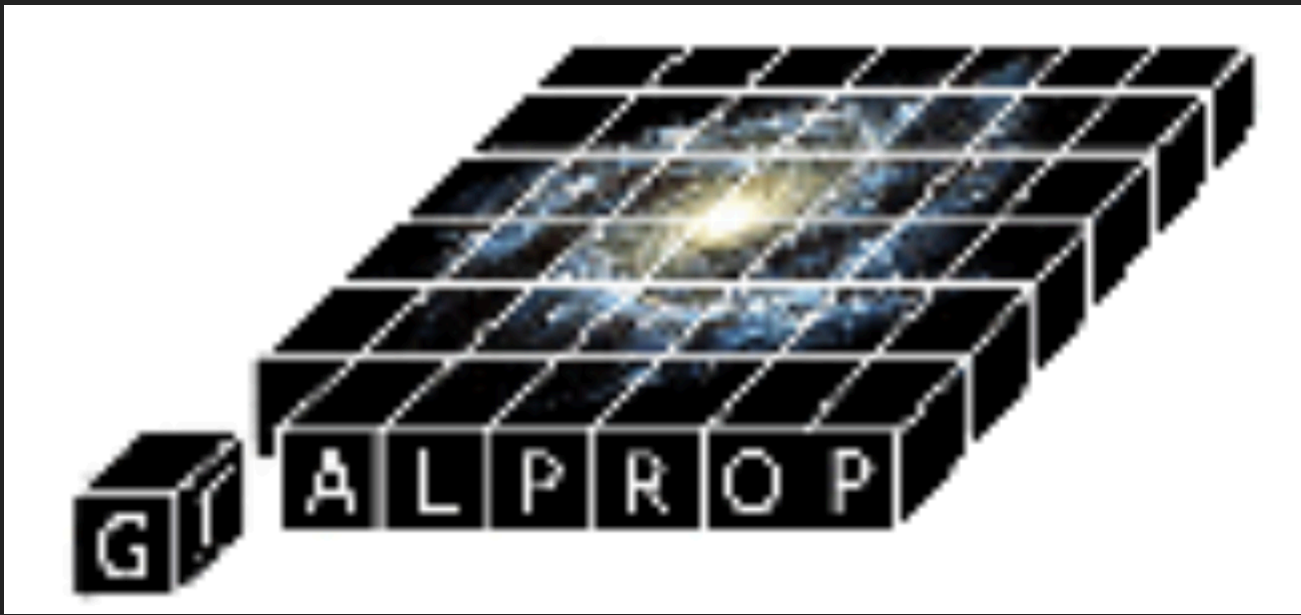
The GALPROP Cosmic-ray Propagation and Nonthermal Emissions Framework: Release v57

T. A. Porter[1] , G. Jóhannesson[2] , and I. V. Moskalenko[1]

[1] W.W. Hansen Experimental Physics Laboratory and Kavli Institute for Particle Astrophysics and Cosmology, Stanford University, Stanford, CA 94305, USA
tporter@stanford.edu

[2] Science Institute, University of Iceland, IS-107 Reykjavik, Iceland

Abstract

The past decade has brought impressive advances in the astrophysics of cosmic rays (CRs) and multiwavelength astronomy, thanks to the new instrumentation launched into space and built on the ground. Modern technologies employed by those instruments provide measurements with unmatched precision, enabling searches for subtle signatures of dark matter and new physics. Understanding the astrophysical backgrounds to better precision than the observed data is vital in moving to this new territory. A state-of-the-art CR propagation code, called GALPROP, is designed to address exactly this challenge. Having 25 yr of development behind it, the GALPROP framework has become a de facto standard in the astrophysics of CRs, diffuse photon emissions (radio to γ-rays), and searches for new physics. GALPROP uses information from astronomy, particle physics, and nuclear physics to predict CRs and their associated emissions self-consistently, providing a unifying modeling framework. The range of its physical validity covers 18 orders of magnitude in energy, from sub-keV to PeV energies for particles and from μeV to PeV energies for photons. The framework and the data sets are public and are extensively used by many experimental collaborations and by thousands of individual researchers worldwide for interpretation of their data and for making predictions. This paper details the latest release of the GALPROP framework and updated cross sections, further developments of its initially auxiliary data sets for models of the interstellar medium that grew into independent studies of the Galactic structure—distributions of gas, dust, radiation, and magnetic fields—as well as the extension of its modeling capabilities. Example applications included with the distribution illustrating usage of the new
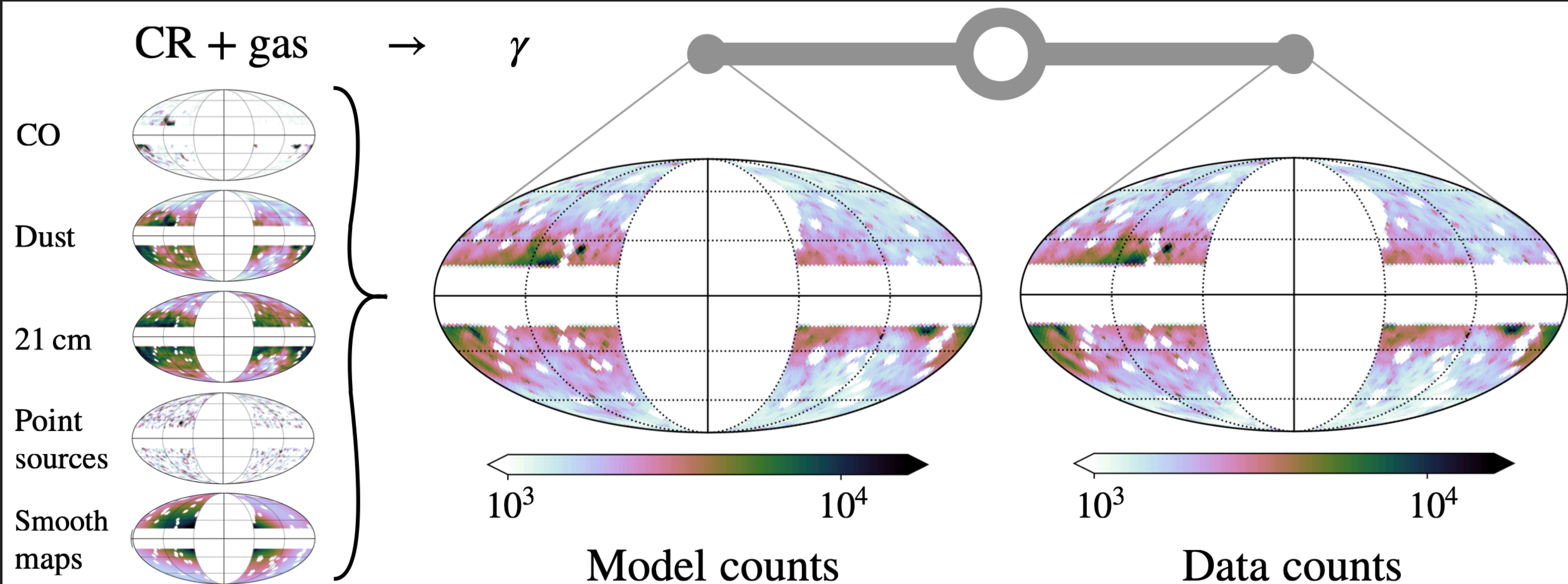
- Target models come from gas and dust tracers.

- CR density comes from Galprop simulations.

- The number of free parameters in cosmic-ray propagation models is already untenable.

(given the relatively limited amount of smooth spectral data)
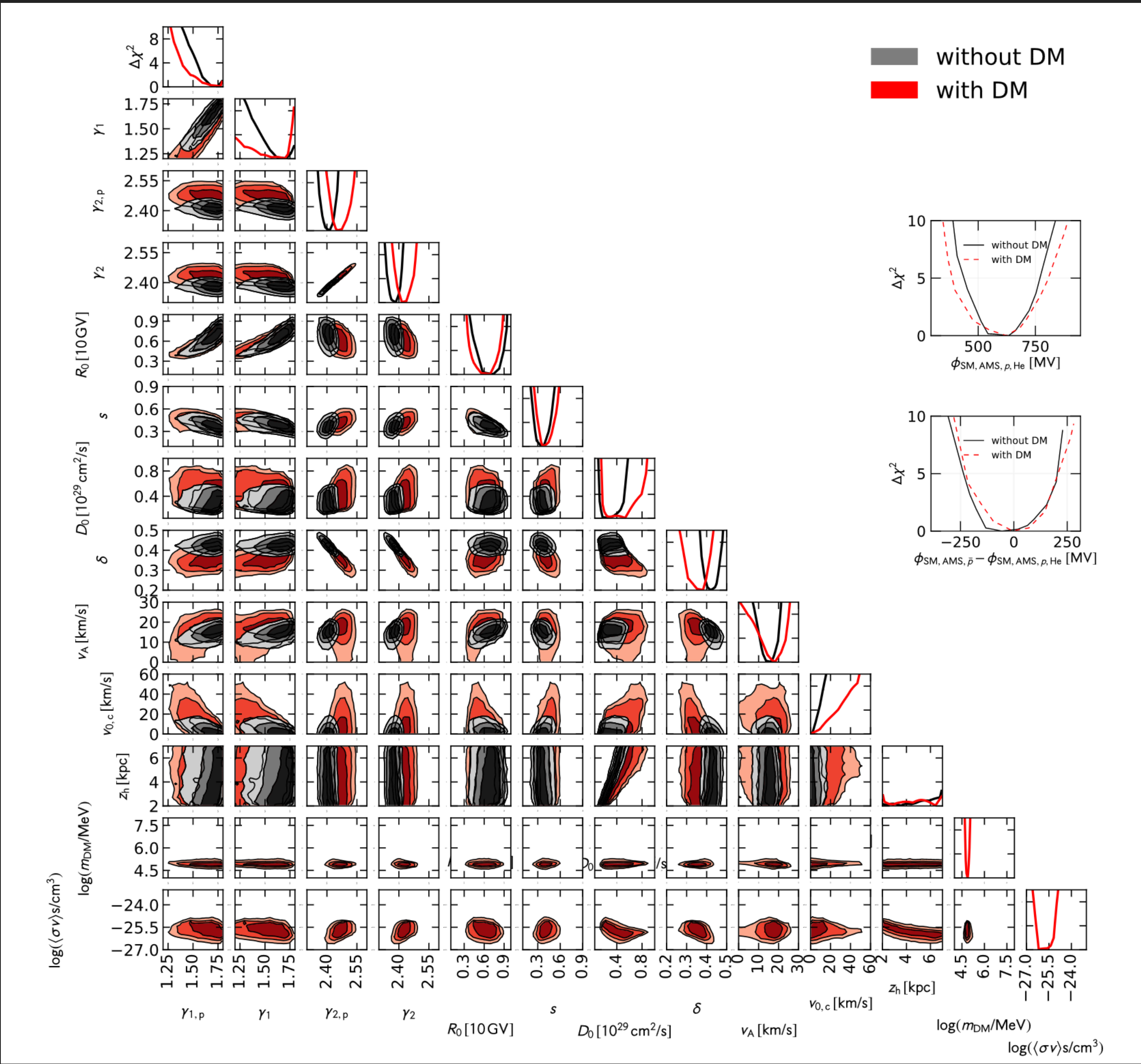
Korsmeier & Cuoco (2016; 1607.06093)

Fit parameters		(uni-PHe)	(uni-PHePbar)	(P)	(PHe)	(main)	(diMauro)	(1GV)	(noVc-1GV)	(noVc-5GV)
$\gamma_{1,p}$		-	-	$1.52^{+0.21}_{-0.32}$	$1.27^{+0.11}_{-0.07}$	$1.36^{+0.07}_{-0.10}$	$1.38^{+0.07}_{-0.10}$	$1.32^{+0.05}_{-0.12}$	$1.61^{+0.06}_{-0.10}$	$1.76^{+0.07}_{-0.04}$
$\gamma_{2,p}$		-	-	$2.52^{+0.12}_{-0.45}$	$2.069^{+0.098}_{-0.069}$	$2.493^{+0.010}_{-0.026}$	$2.499^{+0.026}_{-0.014}$	$2.455^{+0.014}_{-0.007}$	$2.421^{+0.010}_{-0.014}$	$2.454^{+0.026}_{-0.014}$
γ_1		$1.92^{+0.08}_{-0.14}$	$1.50^{+0.07}_{-0.12}$	-	$1.53^{+0.24}_{-0.11}$	$1.29^{+0.04}_{-0.09}$	$1.26^{+0.10}_{-0.06}$	$1.32^{+0.06}_{-0.12}$	$1.65^{+0.07}_{-0.11}$	$1.70^{+0.06}_{-0.07}$
γ_2		$2.582^{+0.010}_{-0.034}$	$2.404^{+0.006}_{-0.022}$	-	$2.003^{+0.094}_{-0.003}$	$2.440^{+0.006}_{-0.018}$	$2.451^{+0.018}_{-0.010}$	$2.412^{+0.012}_{-0.006}$	$2.381^{+0.010}_{-0.010}$	$2.407^{+0.022}_{-0.014}$
R_0	[GV]	$8.16^{+1.22}_{-1.54}$	$8.79^{+1.17}_{-1.55}$	$4.38^{+3.23}_{-1.54}$	$10.5^{+1.40}_{-1.59}$	$5.54^{+0.76}_{-0.54}$	$5.44^{+0.54}_{-0.54}$	$5.52^{+0.33}_{-0.83}$	$7.01^{+0.98}_{-0.54}$	$8.63^{+0.98}_{-0.76}$
s		$0.32^{+0.08}_{-0.02}$	$0.41^{+0.09}_{-0.07}$	$0.48^{+0.16}_{-0.31}$	$0.59^{+0.16}_{-0.04}$	$0.50^{+0.02}_{-0.04}$	$0.50^{+0.05}_{-0.03}$	$0.43^{+0.04}_{-0.03}$	$0.31^{+0.03}_{-0.03}$	$0.32^{+0.04}_{-0.05}$
δ		$0.16^{+0.03}_{-0.02}$	$0.36^{+0.04}_{-0.03}$	$0.29^{+0.46}_{-0.18}$	$0.72^{+0.01}_{-0.11}$	$0.28^{+0.03}_{-0.01}$	$0.27^{+0.02}_{-0.04}$	$0.32^{+0.03}_{-0.02}$	$0.40^{+0.01}_{-0.01}$	$0.36^{+0.02}_{-0.02}$
D_0	[10^{28} cm^2/s]	$2.77^{+2.95}_{-0.53}$	$2.83^{+0.90}_{-0.22}$	$4.78^{+5.22}_{-3.49}$	$5.95^{+0.83}_{-1.37}$	$9.30^{+0.70}_{-5.48}$	$9.04^{+0.96}_{-3.95}$	$8.19^{+1.81}_{-4.68}$	$4.92^{+1.12}_{-2.36}$	$4.60^{+2.71}_{-2.04}$
v_A	[km/s]	$6.80^{+1.18}_{-2.73}$	$29.2^{+2.80}_{-1.47}$	$21.2^{+38.8}_{-21.2}$	$1.84^{+2.36}_{-1.08}$	$20.2^{+3.26}_{-6.33}$	$18.2^{+3.15}_{-5.91}$	$25.0^{+0.92}_{-2.30}$	$22.8^{+1.46}_{-1.05}$	$20.7^{+1.14}_{-3.43}$
$v_{0,c}$	[km/s]	$40.9^{+59.1}_{-5.89}$	$40.2^{+38.1}_{-25.2}$	$5.82^{+94.2}_{-5.82}$	$87.8^{+12.2}_{-24.7}$	$69.7^{+22.0}_{-7.57}$	$57.3^{+41.1}_{-12.3}$	$44.0^{+8.4}_{-16.5}$	-	-
z_h	[kpc]	$3.77^{+3.23}_{-1.77}$	$2.04^{+0.40}_{-0.04}$	$4.22^{+2.78}_{-2.22}$	$6.55^{+0.45}_{-1.63}$	$5.43^{+1.57}_{-3.43}$	$5.84^{+1.16}_{-3.84}$	$6.00^{+1.00}_{-4.00}$	$5.05^{+1.95}_{-3.05}$	$4.12^{+2.88}_{-2.12}$
ϕ_{AMS}		300^{+60}_{-80}	780^{+80}_{-40}	620^{+180}_{-195}	580^{+45}_{-115}	400^{+90}_{-40}	360^{+115}_{-45}	700^{+20}_{-50}	640^{+20}_{-20}	340^{+45}_{-125}
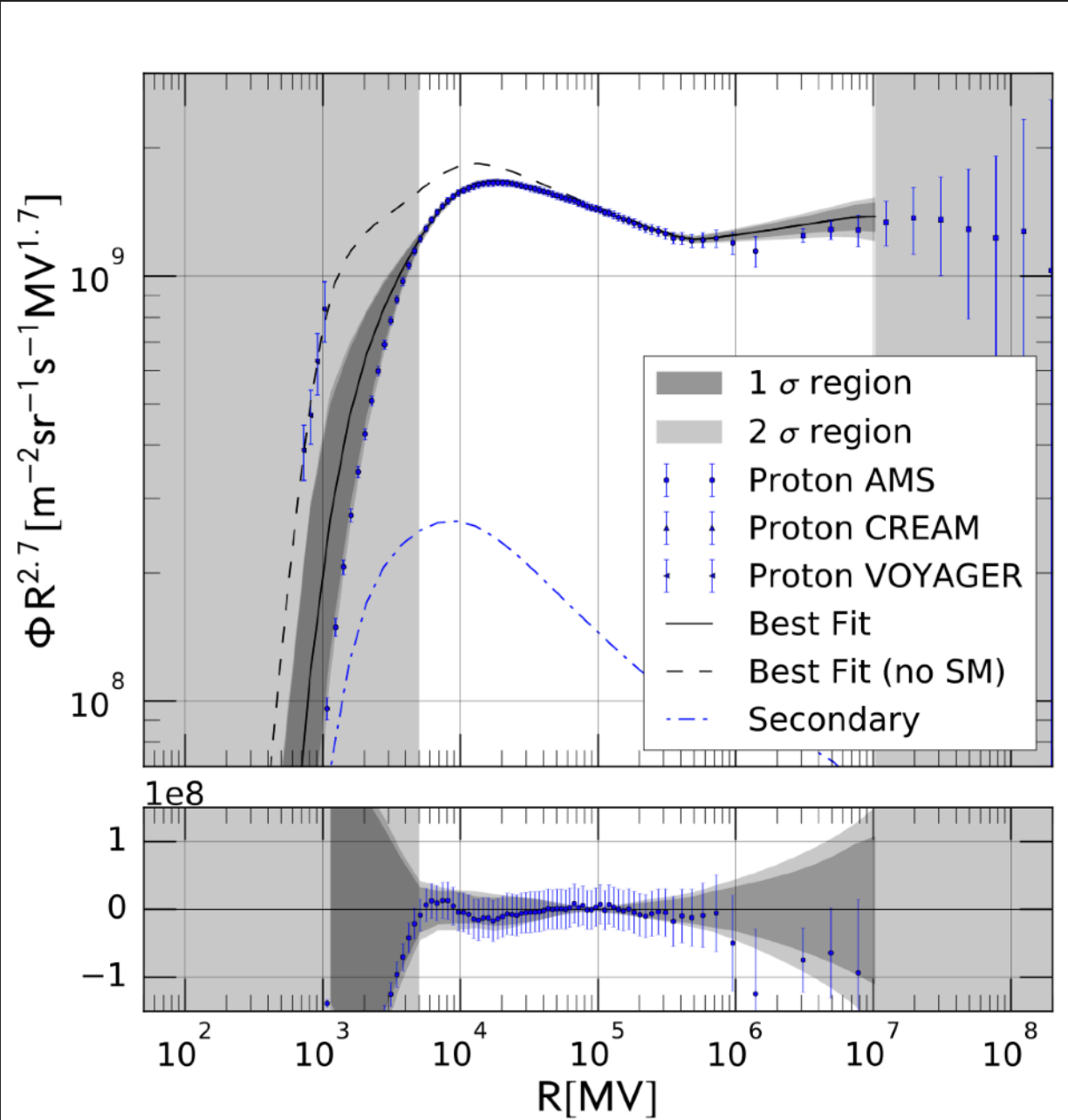
- Assume CR propagation is homogeneous.

- Fit data to local AMS-02 observables.

- It's about the sources.
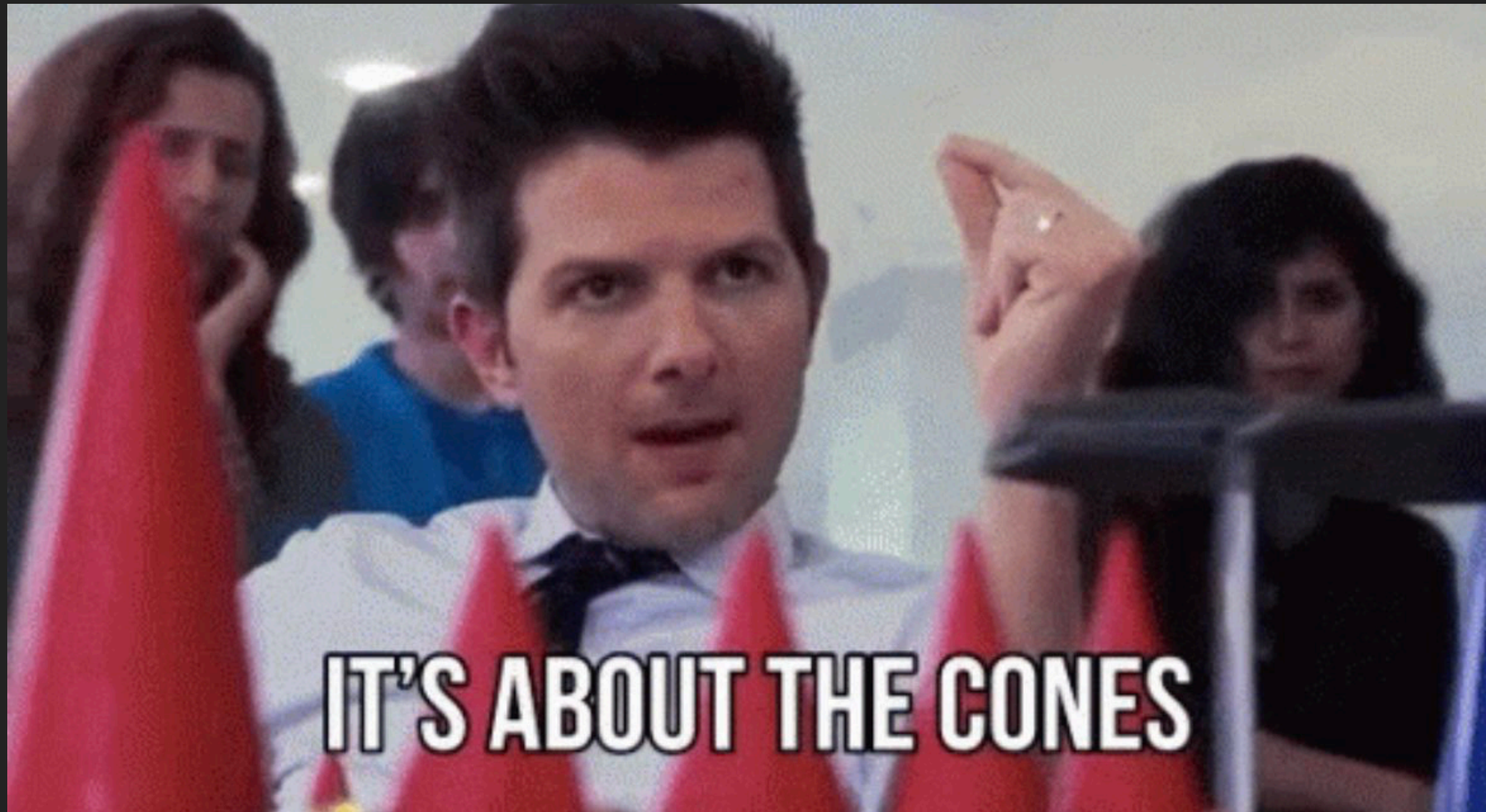
- Pulsars are the sight of observable TeV halos.

- Pulsars are **also** the sight of inhibited cosmic-ray diffusion.

- Can use multi wavelength pulsar information to trace regions with inhibited diffusion!.

$$\frac{\partial \mathcal{W}}{\partial t} + v_A \frac{\partial \mathcal{W}}{\partial z} = (\Gamma_{\mathrm{CR}} - \Gamma_{\mathrm{D}})\mathcal{W}(k, z, t)$$

$$\Gamma_{\mathrm{CR}}(k) = \frac{2\pi}{3} \frac{c|v_A|}{k\mathcal{W}(k)\,U_0} \left[p^4 \frac{\partial f}{\partial z} \right]_{p_{\mathrm{res}}}$$
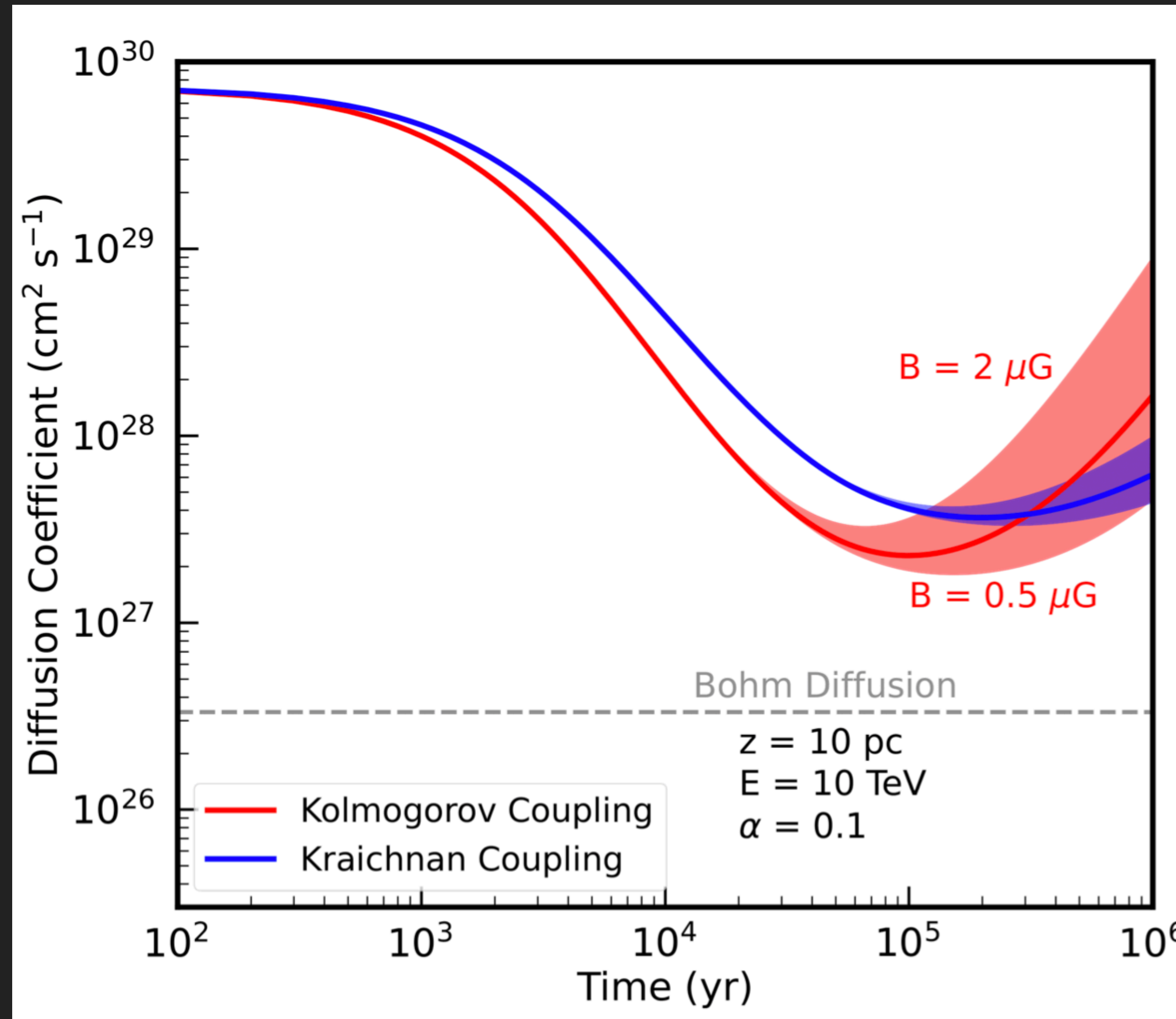
- Many uncertainties in these models:

  - Role of Supernova Remnant

  - **Disruption by molecular gas or magnetic fields**

  - Pulsar Proper Motion

  - 1D vs. 3D diffusion

  - non-Resonant Terms

  - Halos in close proximity
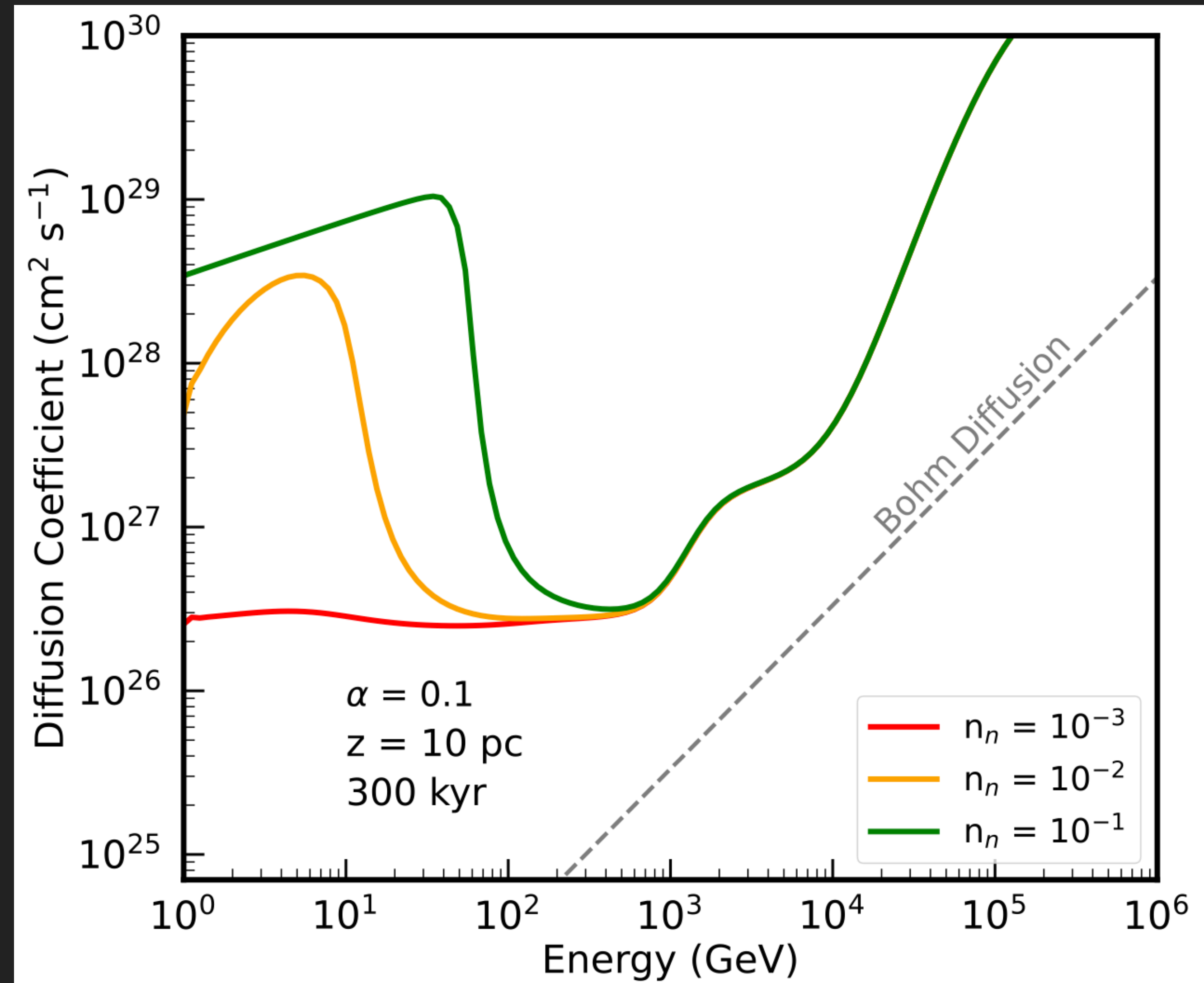
OPEN QUESTION: MSP HALOS?

▸ Do MSPs Have TeV Halos?

▸ Tentative: **4.24σ** Poisson evidence from a HAWC stacking analysis (~**2.3σ** from blank sky test).

▸ Possible MSP Detection by LHAASO

▸ Important theoretical implications:

    ▸ Cosmic-Ray confinement near pulsars?

    ▸ Cosmic-Ray diffusion at high latitudes

    ▸ PWN/Magnetospheric acceleration models.
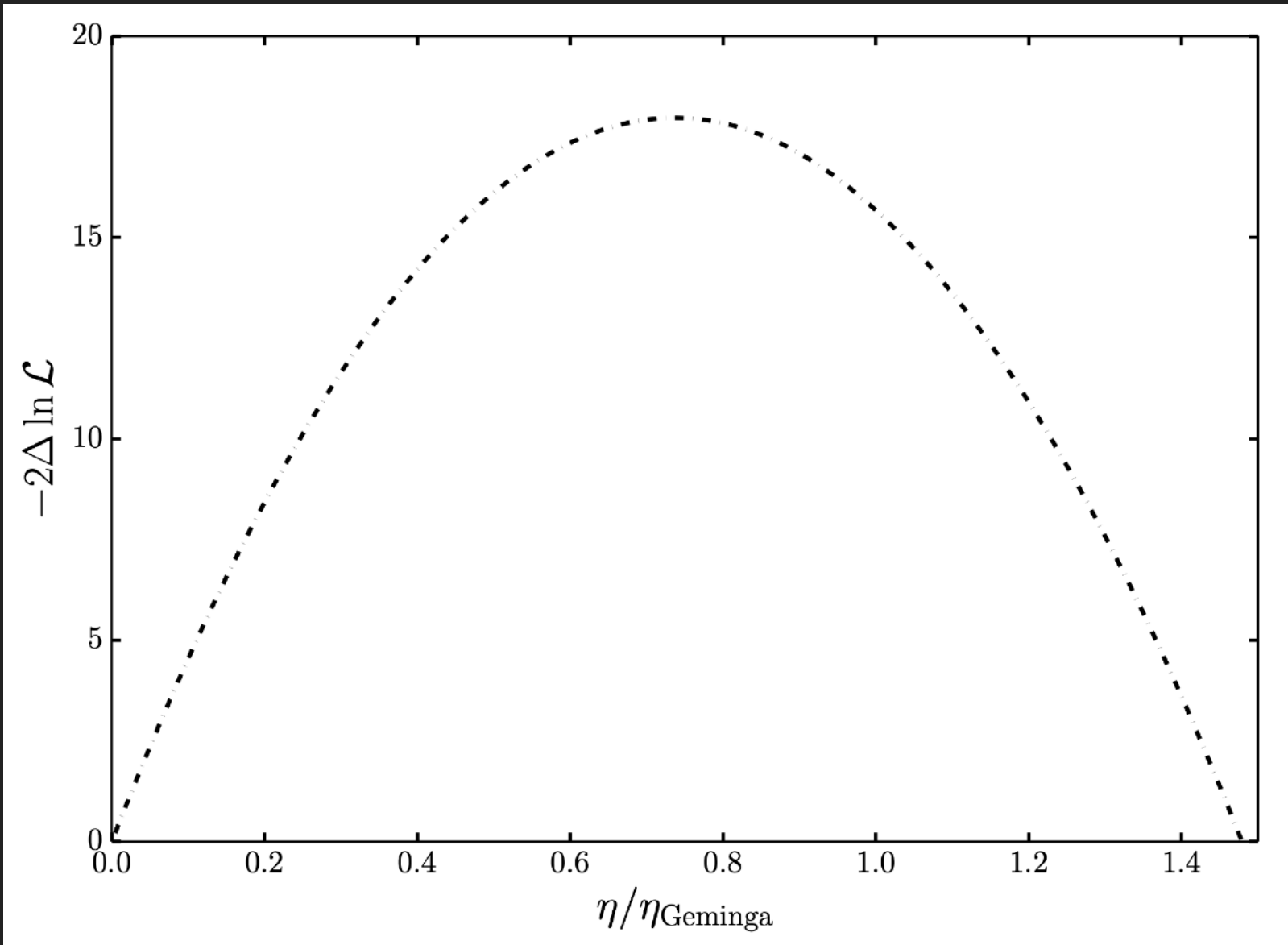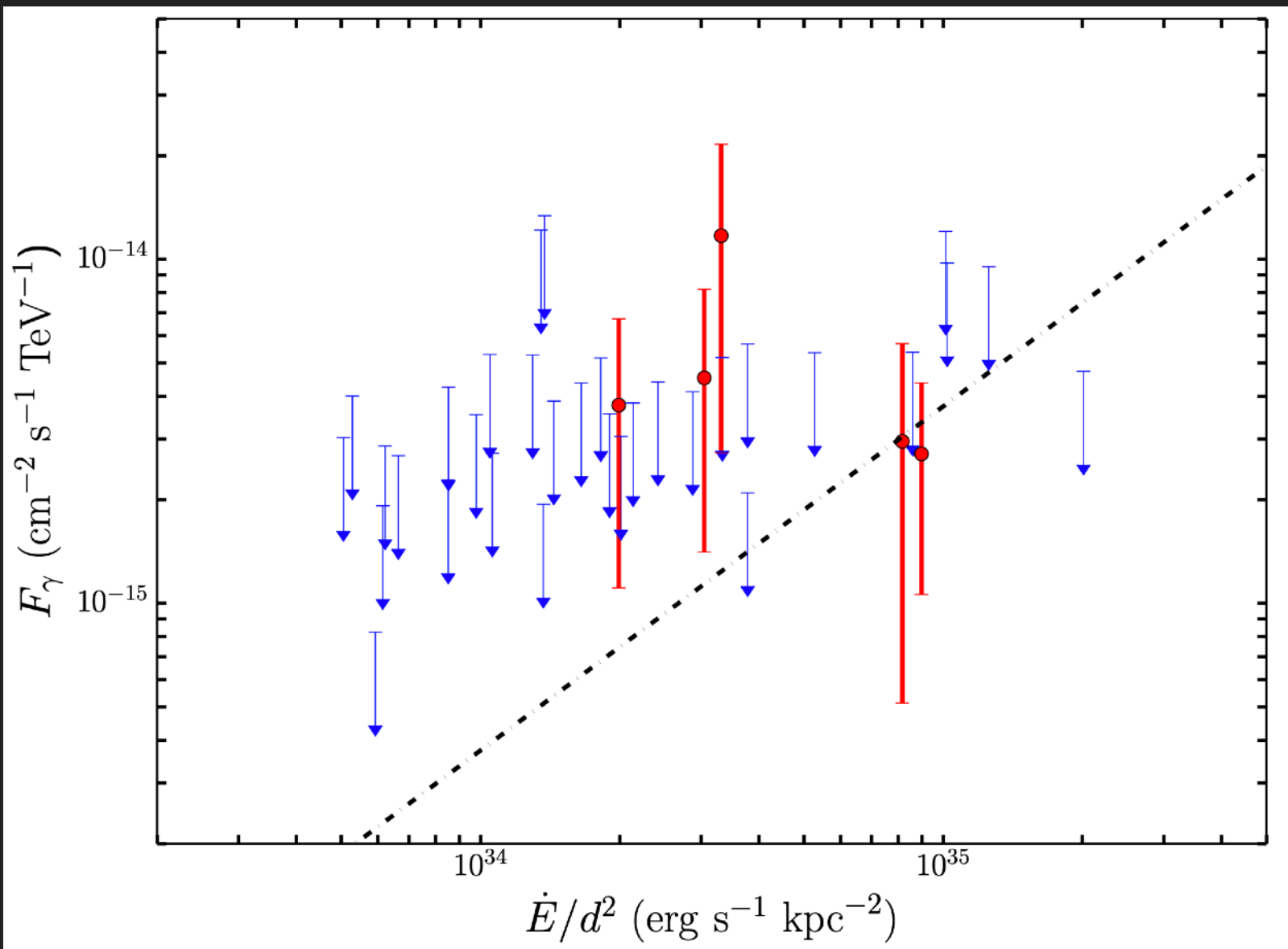
LHAASO Collaboration (2023; 2305.17030)

| 1LHAASO J0216+4237u | 0.33 | ATNF PSR J0218+4232 | $\dot{E} = 2.44 \times 10^{35}$ erg s^{-1}, $\tau_c = 476000.0$ kyr, $d = 3.15$ kpc |
| | 0.33 | 4FGL J0218.1+4232 | PSR J0218+4232; MSP; |

TEV HALOS SOLVE COSMIC-RAY DIFFUSION

▸ Pulsar catalogs provide an answer:

  ▸ >3000 pulsars

  ▸ Specific locations, ages, and spin down powers

  ▸ Translates directly into local diffusion model in streaming instability models.

#	PSRJ	P0 (s)	P1	DIST (kpc)	AGE (Yr)	BSURF (G)	EDOT (ergs/s)
1	J0537−6910	0.016122	5.18e−14	49.700	4.93e+03	9.25e+11	4.88e+38
2	J0534+2200	0.033392	4.21e−13	2.000	1.26e+03	3.79e+12	4.46e+38
3	J0540−6919	0.050570	4.79e−13	49.700	1.67e+03	4.98e+12	1.46e+38
4	J1813−1749	0.044741	1.27e−13	4.700	5.58e+03	2.41e+12	5.60e+37
5	J1400−6325	0.031182	3.89e−14	7.000	1.27e+04	1.11e+12	5.07e+37
6	J1747−2809	0.052153	1.56e−13	8.141	5.31e+03	2.88e+12	4.33e+37
7	J1833−1034	0.061884	2.02e−13	4.100	4.85e+03	3.58e+12	3.37e+37
8	J2022+3842	0.048579	8.61e−14	10.000	8.94e+03	2.07e+12	2.96e+37
9	J0205+6449	0.065716	1.94e−13	3.200	5.37e+03	3.61e+12	2.70e+37
10	J2229+6114	0.051624	7.83e−14	3.000	1.05e+04	2.03e+12	2.25e+37
11	J1513−5908	0.151582	1.53e−12	4.400	1.57e+03	1.54e+13	1.73e+37
12	J1617−5055	0.069357	1.35e−13	4.743	8.13e+03	3.10e+12	1.60e+37
13	J1124−5916	0.135477	7.53e−13	5.000	2.85e+03	1.02e+13	1.19e+37
14	J1930+1852	0.136855	7.51e−13	7.000	2.89e+03	1.03e+13	1.16e+37
15	J1023−5746	0.111472	3.84e−13	2.080	4.60e+03	6.62e+12	1.09e+37
16	J1420−6048	0.068180	8.32e−14	5.632	1.30e+04	2.41e+12	1.04e+37
17	J1410−6132	0.050052	3.20e−14	13.510	2.48e+04	1.28e+12	1.01e+37
18	J1849−0001	0.038523	1.42e−14	*	4.31e+04	7.47e+11	9.78e+36
19	J1402+13	0.005890	4.83e−17	*	1.93e+06	1.71e+10	9.34e+36
20	J1846−0258	0.326571	7.11e−12	5.800	7.28e+02	4.88e+13	8.06e+36
21	J0835−4510	0.089328	1.25e−13	0.280	1.13e+04	3.38e+12	6.92e+36
22	J1811−1925	0.064667	4.40e−14	5.000	2.33e+04	1.71e+12	6.42e+36
23	J1111−6039	0.106670	1.95e−13	*	8.66e+03	4.62e+12	6.35e+36
24	J1813−1246	0.048072	1.76e−14	2.635	4.34e+04	9.30e+11	6.24e+36
25	J1838−0537	0.145708	4.72e−13	*	4.89e+03	8.39e+12	6.02e+36
26	J1838−0655	0.070498	4.92e−14	6.600	2.27e+04	1.89e+12	5.55e+36
27	J1418−6058	0.110573	1.69e−13	1.885	1.03e+04	4.38e+12	4.95e+36
28	J1935+2025	0.080118	6.08e−14	4.598	2.09e+04	2.23e+12	4.66e+36
29	J1856+0245	0.080907	6.21e−14	6.318	2.06e+04	2.27e+12	4.63e+36
30	J1112−6103	0.064962	3.15e−14	4.500	3.27e+04	1.45e+12	4.53e+36
31	J1640−4631	0.206443	9.76e−13	12.750	3.35e+03	1.44e+13	4.38e+36
32	J1844−0346	0.112855	1.55e−13	*	1.16e+04	4.23e+12	4.25e+36
33	J1952+3252	0.039531	5.84e−15	3.000	1.07e+05	4.86e+11	3.74e+36
34	J1826−1256	0.110224	1.21e−13	1.550	1.44e+04	3.70e+12	3.58e+36
35	J1709−4429	0.102459	9.30e−14	2.600	1.75e+04	3.12e+12	3.41e+36
36	J2021+3651	0.103741	9.57e−14	1.800	1.72e+04	3.19e+12	3.38e+36
37	J1524−5625	0.078219	3.90e−14	3.378	3.18e+04	1.77e+12	3.21e+36
38	J1357−6429	0.166108	3.60e−13	3.100	7.31e+03	7.83e+12	3.10e+36
39	J1913+1011	0.035909	3.37e−15	4.613	1.69e+05	3.52e+11	2.87e+36
40	J1826−1334	0.101487	7.53e−14	3.606	2.14e+04	2.80e+12	2.84e+36

Pulsar searches and timing with the square kilometre array

R. Smits[1], M. Kramer[1], B. Stappers[1], D. R. Lorimer[2,3], J. Cordes[4], and A. Faulkner[1]

[1] Jodrell Bank Centre for Astrophysics, University of Manchester, UK
   e-mail: `Roy.Smits@manchester.ac.uk`
[2] Department of Physics, 210 Hodges Hall, West Virginia University, Morgantown, WV 26506, USA
[3] National Radio Astronomy Observatory, Green Bank, USA
[4] Astronomy Department, Cornell University, Ithaca, NY, USA

ABSTRACT

The square kilometre array (SKA) is a planned multi purpose radio telescope with a collecting area approaching 1 million square metres. One of the key science objectives of the SKA is to provide exquisite strong-field tests of gravitational physics by finding and timing pulsars in extreme binary systems such as a pulsar-black hole binary. To find out how three preliminary SKA configurations will affect a pulsar survey, we have simulated SKA pulsar surveys for each configuration. We estimate that the total number of pulsars the SKA will detect, is around 14 000 normal pulsars and 6000 millisecond pulsars, using only the 1-km core and 30-mn integration time. We describe a simple strategy for follow-up timing observations and find that, depending on the configuration, it would take 1–6 days to obtain a single timing point for 14 000 pulsars. Obtaining one timing point for the high-precision timing projects of the SKA, will take less than 14 h, 2 days, or 3 days, depending on the configuration. The presence of aperture arrays will be of great benefit here. We also study the computational requirements for beam forming and data analysis for a pulsar survey. Beam forming of the full field of view of the single pixel feed 15 m dishes using the 1-km core of the SKA requires about 2.2×10^{15} operations
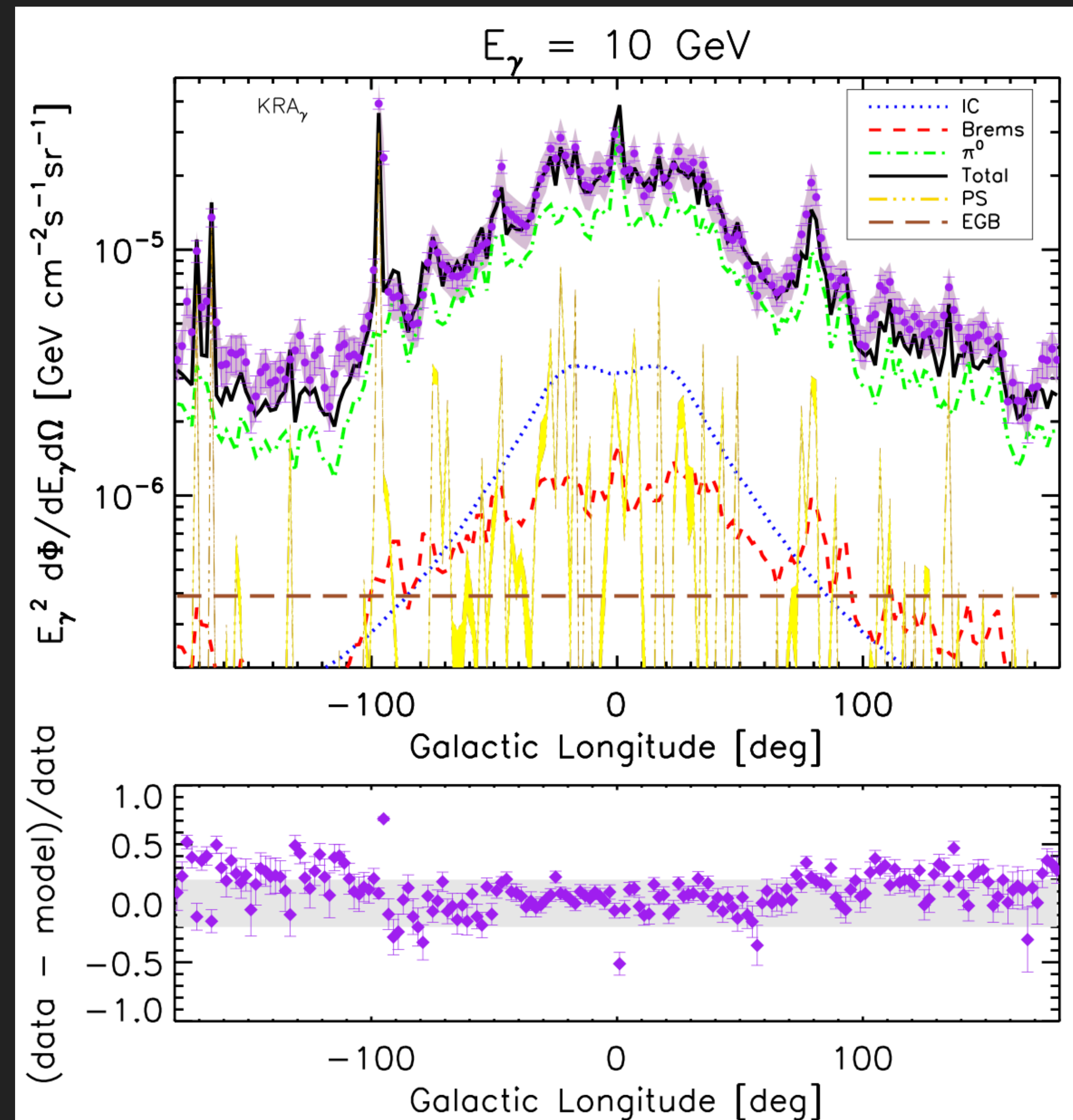
▸ First attempts at this approach.

▸ Decreasing diffusion in the spiral arms produces better fits to GeV gamma-ray data
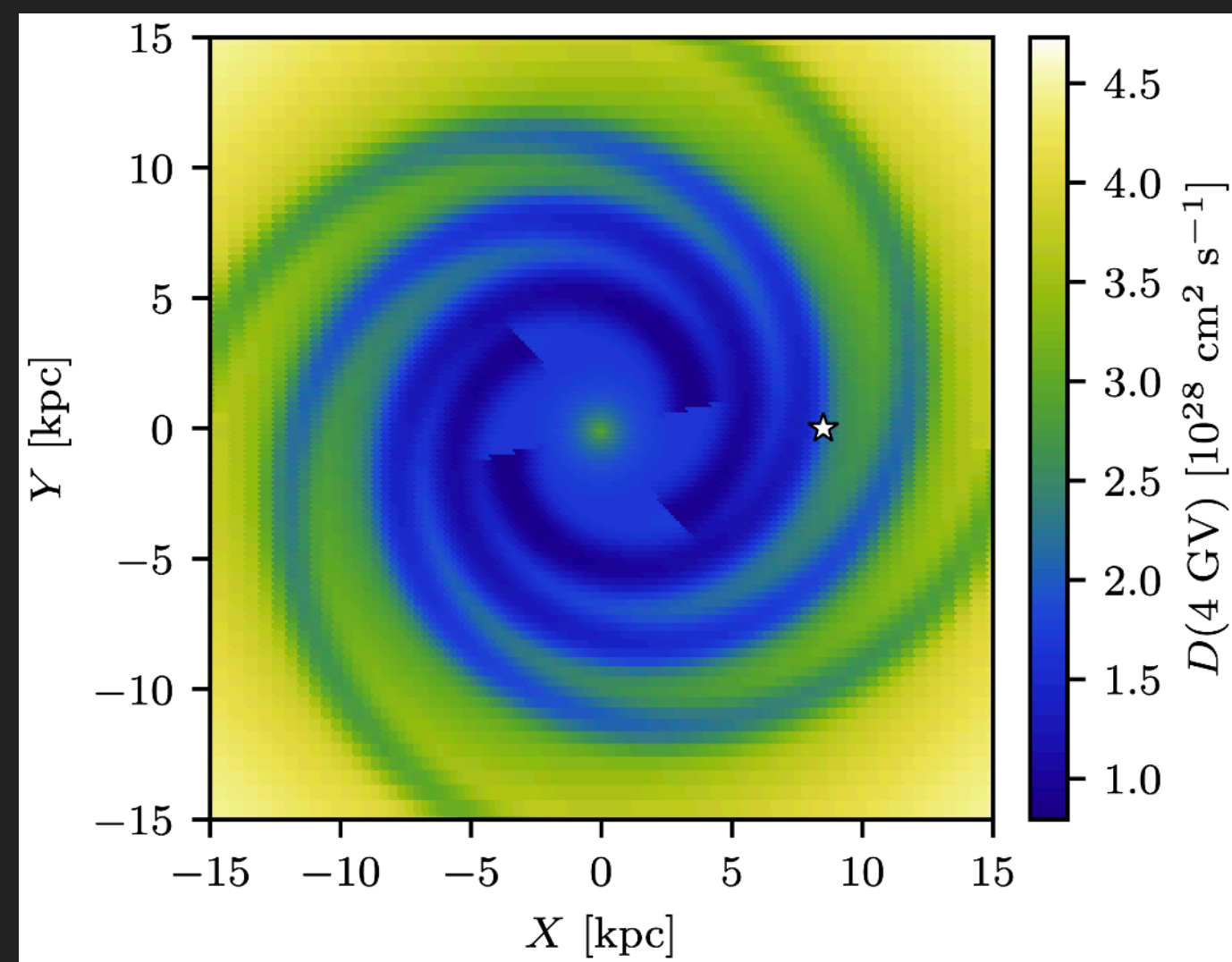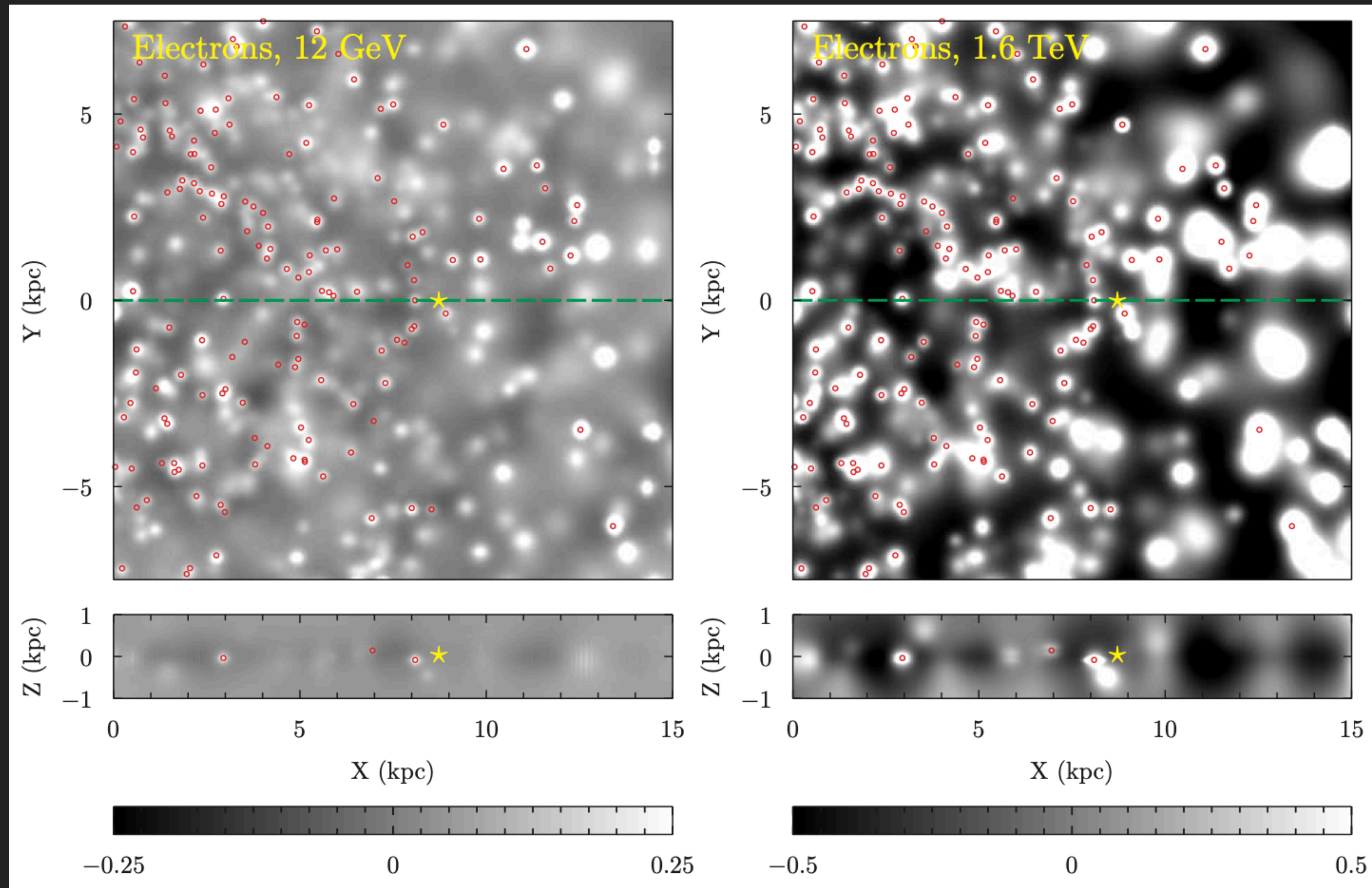
Jóhannesson et al. (2019.1903.05509)

TEV HALOS SOLVE COSMIC-RAY DIFFUSION

Porter et al. (2019; 1909.02223)
See also: Thaler et al. (2022 2209.02295)

▸ TeV halos are everywhere, and an important component of TeV sources and diffuse emission.

▸ Standard methods of building a diffuse model fail at TeV scales.

▸ The solution is the sources

  ▸ Radio/Gamma-Ray Observations of Pulsars

  ▸ Theoretical models to transfer information about pulsar age/spindown power/ environment into information about local diffusion.

  ▸ Computational models of cosmic-ray diffusion in inhomogeneous media (see Thaler et al. 2022)